Department of Chemical and Metallurgical Engineering

The use of alternative reductants in pyrometallurgical operations

Desmond Attah-Kyei

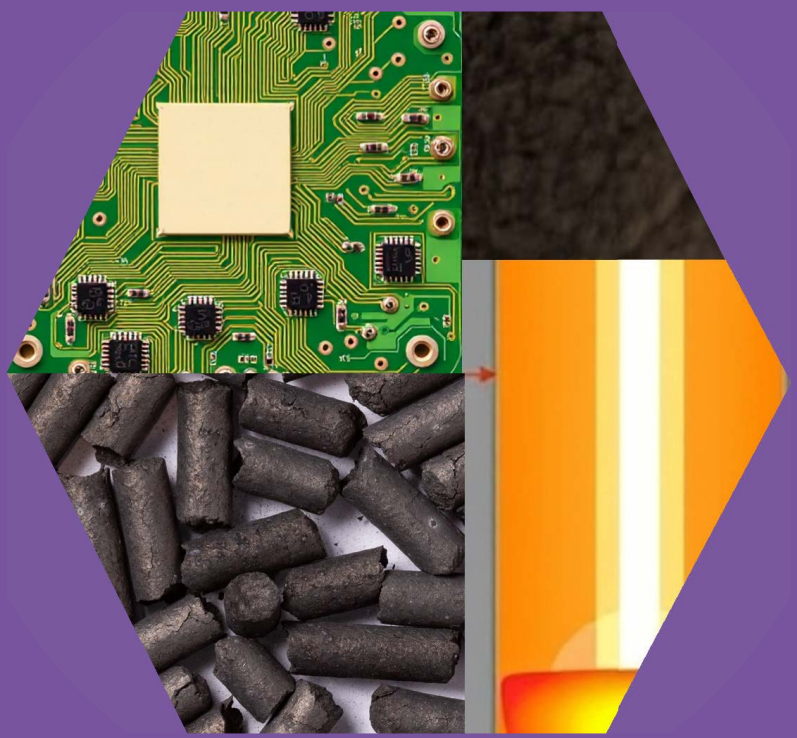

Aalto University

DOCTORAL THESES

Aalto University publication series
DOCTORAL THESES 283/2024

The use of alternative reductants in pyrometallurgical operations

Desmond Attah-Kyei

A doctoral thesis completed for the degree of Doctor of Science (Technology) to be defended, with the permission of the Aalto University School of Chemical Engineering, at a public examination held at the Circular Raw Materials Hub, C100 Aluminium of the school on 31 January 2025 at 12:00.

Aalto University
School of Chemical Engineering
Department of Chemical and Metallurgical Engineering
Metallurgical Thermodynamics and Modelling

Supervising professor
Professor Daniel Lindberg, Aalto University, Finland

Thesis advisors
Professor Daniel Lindberg, Aalto University, Finland
Professor Ari Jokilaakso, Aalto University, Finland

Preliminary examiners
Professor Caisa Samuelsson, Luleå University of Technology, Sweden
Professor Merete Tangstad, Norwegian University of Science and Technology, Norway

Opponent
Professor Caisa Samuelsson, Luleå University of Technology, Sweden

Aalto University publication series
DOCTORAL THESES 283/2024

ISBN 978-952-64-2209-1 (printed)
ISBN 978-952-64-2210-7 (pdf)
ISSN 1799-4934 (printed)
ISSN 1799-4942 (pdf)
http://urn.fi/URN:ISBN:978-952-64-2210-7

Unigrafia Oy
Helsinki 2024

Finland

NORDIC SWAN ECOLABEL
Printed matter
4041-0619

Author
Desmond Attah-Kyei

Name of the doctoral thesis
The use of alternative reductants in pyrometallurgical operations

Publisher School of Chemical Engineering

Unit Department of Chemical and Metallurgical Engineering

Series Aalto University publication series DOCTORAL THESES 283/2024

Field of research

Manuscript submitted 14 August 2024 **Date of the defence** 31 January 2025

Permission for public defence granted (date) 20 November 2024 **Language** English

☐ **Monograph** ☒ **Article thesis** ☐ **Essay thesis**

Abstract

Due to the rising concern about climate change in the last few decades, the metallurgical industry is moving toward greener practices. This move is driven by pressing concerns about the reduction of greenhouse gas emissions and environmental footprints of industrial activities. One of the main strategies in this transition is to employ alternative reductants in high temperature processes. Substituting traditional reductants like coal or coke with sustainable alternatives such as hydrogen or biochar minimizes the carbon emission and provides economic benefits in addition.

In this thesis work, several non-fossil reductants were applied in high temperature processes for metal recovery from secondary sources. Leach residue of printed circuit board (PCB) was employed as reductant for solid-state reduction of hematite in DSC-TGA coupled with QMS. Hydrogen was utilized in the reduction of zinc leach residue while nickel and copper smelting slag reduction were treated with biochar on laboratory scale in a vertical fur-nace. The feasibility of adopting alternative reductants in ironmaking and pyrometallurgical treatment of secondary resources were determined in this study. The effect of the amount of reducing agent, reduction time, and temperature on the extent of reduction was investigated.

The studies revealed that although PCB leach residue can be applied in reduction processes, it can only partially replace conventional reductants. PCB was also found to be effective at lower temperatures (< 1000 ^{0}C). Leach residue from zinc processing were reduced with hydrogen at temperatures of 1200 ^{0}C, 1250 ^{0}C, and 1300 ^{0}C using H_2 and N_2 gases to form the reducing gas atmosphere. The results showed that H_2 is an effective reductant because reduction proceeded rapidly, forming speiss droplets within the slag already after 10 minutes. Nickel and copper smelting slags were reacted with biochar which were produced from hydrolysis lignin and black pellet biomass by pyrolysis at 600 and 1200 °C, and with metallurgical coke for comparison. Nickel reduction experiments were done at 1400 °C for 15, 30, and 60 min under inert gas atmosphere. The samples were quickly quenched and analyzed with Electron Probe X-ray Microanalysis. The results showed that the use of biochar resulted in faster reaction kinetics in the reduction process compared to coke. Copper slag reduction experiments were performed at 1250, 1300 and 1350 °C for 60 min in order to investigate the effect of temperature and the effect of time on reduction progress was studied at 1250 °C for 15, 30 and 60 min. The results revealed that reduction rapidly progresses to the formation of metal alloy within 10 min. Valuable metals like copper and nickel were reduced to the metal phase.

Thermodynamic simulations were performed with FactSage™ at the experimental conditions and compared with results from the lab scale experiments. FactSage™ predictions were in agreement with the experiments.

Keywords Alternative reductants, Secondary resources, Thermodynamic modeling, Metal recovery

ISBN (printed) 978-952-64-2209-1 **ISBN (pdf)** 978-952-64-2210-7

ISSN (printed) 1799-4934 **ISSN (pdf)** 1799-4942

Location of publisher Helsinki **Location of printing** Helsinki **Year** 2024

Pages 138 **urn** http://urn.fi/URN:ISBN:978-952-64-2210-7

Acknowledgements

This thesis marks the culmination of the research work conducted at Aalto University School of Chemical engineering in Metallurgical thermodynamics and modeling research group. The work in Aalto University started in 2019 but the official doctoral study right was obtained in November 2019. This research work in this thesis would not have been possible without funding by Business Finland (SYMMET and TOCANEM projects).

I would like to first and foremost express my gratitude to my supervisor, Professor Daniel Lindberg for his unwavering support, insightful guidance, and constant encouragement. I first met Prof. Lindberg in 2018 when he was still at Åbo Akademi University. Then I was a Masters' student at Stellenbosch University. I came to Åbo Akademi to perform some experiments regarding my maters' thesis. Daniel was helpful in the planning and execution of the experiments. Before I went back to South Africa, I expressed my interest on working with him for my PhD research which he readily accepted. After moving to Aalto, I started my doctoral studies under his supervision.

My deep appreciation to Lassi who trained me to use most of the equipment in the lab and was readily to assist and to share his broad knowledge about everything and gave quick comment on the manuscripts. I am also grateful to Professor emeritus Pekka Taskinen who shared his valuable experience and knowledge during the research. Special thanks to Professor Ari Jokilaakso for his contribution to my doctoral studies. I am also indebted to the co-authors of the published articles including Dr Dmitry Sukhomlinov, Dr Justin Salminen, Dr Radoslaw Michallik, Dr Mia Tiljander, Dr Fiseha Tesfaye as well as my colleagues Junmo, David, Minna, Fabiola, Wildu and everyone else I was privileged to work with.

My PhD journey would have been extremely difficult had it not been for the support of my lovely daughter, Kristodea and dear wonderful wife, Grace, who have provided much-needed balance and perspective. Your understanding and encouragement have helped me navigate the challenges of this journey with resilience and optimism. Your sacrifice has made my achievements possible.

Last and the most important, I want to thank God for His help and direction in this journey. I am forever grateful for everything You have done for me. Indeed, I am what I am by the grace of the Almighty God.

Espoo, November 2024
Desmond Attah-Kyei

Contents

List of Abbreviations and Symbols

BF	Blast furnace
BOF	Basic oxygen furnace
CCS	Carbon capture and storage
COG	Coke oven gas
DSC	Differential scanning calorimeter
EDS	Energy dispersive X-ray spectrometer
EPMA	Electron probe microanalysis
e-waste	Electronic waste
GHGs	Greenhouse gasses
ICP-OES	Inductively coupled plasma - optical emission spectroscopy
$L^{metal/slag}$	Distribution coefficient of element between metal alloy and slag
LA-ICP-MS	Laser ablation-inductively coupled plasma-mass spectrometry
Me	Metal
MeO	Metal oxide
MF	Metallic fractions
Mt	Million tonnes
NMF	Non-metallic fractions
PCB	Printed circuit board
QMS	Quadrupole mass spectrometer
SEM	Scanning electron microscope
SMR	Steam methane reforming
T	Tonne
TGA	Thermogravimetric analyzer

wt%	Weight percent
XRD	X-ray diffraction
XRF	X-ray fluorescence

List of Publications

This doctoral dissertation consists of a summary and of the following publications which are referred to in the text by their Roman numerals I-IV.

I. Attah-Kyei, D., Akdogan, G., Dorfling, C., Zietsman, J., Lindberg, D., Tesfaye, F., Reynolds, Q., 2020. Investigation of waste PCB leach residue as a reducing agent in smelting processes. Miner. Eng. 156. https://doi.org/10.1016/j.mineng.2020.106489.

II. Attah-Kyei, D., Klemettinen, L., Michallik, R., Salminen, J., Taskinen, P., Lindberg, D., 2022. Hydrogen as Carbon-Free Reducing Agent in Non-ferrous Slag Fuming. Metallurgical and Materials Transactions B: Process Metallurgy and Materials Processing Science 53(6). https://doi.org/10.1007/s11663-022-02640-0.

III. Attah-Kyei, D., Sukhomlinov, D., Tiljander, M., Klemettinen, L., Taskinen, P., Jokilaakso, A., Lindberg, D., 2023. A Crucial Step Toward Carbon Neutrality in Pyrometallurgical Reduction of Nickel Slag. Journal of Sustainable Metallurgy. 9, 1759-1776 https://doi.org/10.1007/s40831-023-00763-5

IV. Attah-Kyei, D., Sukhomlinov, D., Klemettinen, L., Michallik, R., O'Brien, H., Taskinen, P., Lindberg, D., 2024. Pyrometallurgical Reduction of Copper Slag with Biochar for Metal Recovery. Journal of Sustainable Metallurgy. https://doi.org/10.1007/s40831-024-00885-4

Author's Contribution

Publication I: Investigation of waste PCB leach residue as a reducing agent in smelting processes

GA and CD designed the experiments. The main author, DA, performed thermodynamic modeling with the help of JZ and DL, conducted the experiments and the analysis of the experimental samples together with QR, wrote the first draft of the manuscript, modified it together with FT, and revised it according to the comments from all the authors.

Publication II: Hydrogen as Carbon-Free Reducing Agent in Non-ferrous Slag Fuming

DA and LK designed the experimental plan together with DL and PT. DA conducted the experiments and analysis of samples with LK. JS offered valuable insight in the interpretation of results along with DL and PT. RM conducted the EPMA analyses of the samples. DA performed the thermodynamic calculations together with DL. DA wrote the first draft of the manuscript, and all the authors gave valuable input to the published version. DL supervised the work and provided funding.

Publication III: A Crucial Step Toward Carbon Neutrality in Pyrometallurgical Reduction of Nickel Slag

DA defined the research plan through discussion with DS, PT, and AJ. DA performed the experiments with assistance from DS and analysis of experimental samples by SEM-EDS. DA performed the thermodynamic calculations with input from DL. MT provided valuable help during the analysis of samples with EPMA. LK offered valuable input on the interpretation of the results. DA wrote the first draft and modified it according to comments from the co-authors.

Publication IV: Pyrometallurgical Reduction of Copper Slag with Biochar for Metal Recovery

The main author, DA, designed the research, and conducted the experiments and SEM analysis on the experimental samples. RM performed the EPMA characterization of the samples with assistance from DA, LK and HO performed the LA-ICP-MS analyses. The results were interpreted through discussions with DS, PT, and DL. DA performed the thermodynamic calculations with input from DL. DA wrote the first draft and revised the manuscript based on the input from all the co-authors.

1. Introduction

In the last few decades, concerns about climate change have considerably increased as global temperatures are on the rise. Climate change is considered to be one of the most critical environmental challenges faced by the world. There are predictions that, if human activities responsible for emissions remain unchanged, the average temperature in the world will increase by 1.4 -5.8 ℃. This would result in serious repercussions for humans and the environment. The increasing use of fossil fuels in metallurgical processes is a major contributing factor to greenhouse gas (GHG) emissions, which plays a key role in climate change [1]

To mitigate GHG emissions, the European Commission has presented a long-term strategic vision that explores possible ways of moving to net-zero GHG emissions by 2050. The strategy explores ways to reduce these gasses in key economic sectors including energy, transport, industry, and agriculture, based on existing and emerging technological solutions. As part of the goal to make the EU climate-neutral by 2050, EU countries must cut emissions of GHGs by at least 55% by 2030 compared to 1990 levels [2, 3]. A global effort, known as the Kyoto Protocol, was developed to reduce emissions by establishing legally enforceable limits on GHG emissions for industrialized countries. The Kyoto Protocol took effect on February 16, 2005, and by July 2006, 164 nations had consented to the agreement that accounted for over 60% of emissions from industrialized nations [4]. In fact, the agreement reached at the 2015 United Nations Climate Change Conference states that, to restrict the rise in global temperatures to less than 2 ℃ compared to pre-industrial levels, atmospheric CO2 concentrations must be limited to less than 450 ppm by the year 2100 [5].

It has been reported that the metal industry, especially the iron and steel industry, is responsible for nearly 10% of industrial CO_2 emissions in the world, releasing close to 650 Mt of CO_2 per annum. Presently, approximately 73% of global steel production is carried out using the coke- or coal-based blast furnace-basic oxygen furnace route (BF-BOF) [5, 6, 7]. One of the main contributing factors is the metallurgical industry's dependence on coking coal resources [8]. To minimize the emission of CO_2 and other GHGs to the environment, the implementation of innovative technologies or the use of non-fossil reductants and fuels has become more attractive, as this would radically mitigate the environmental crisis associated with greenhouse gas emissions and diminish the reliance on fossil fuels. Some metallurgy companies, including Makeevka steel in Ukraine and Solmer steel in France, use hydrogen-rich coke oven gas (COG) in the BF. Hydrogen metallurgy, where hydrogen or hydrogen-rich gas are used to reduce metal oxide to metal has gained traction nowadays. Given that hydrogen may be obtained from non-fossil sources, carbon capture and storage (CCS) technology may be incorporated in hydrogen metallurgy to effectively decrease CO_2 emissions [7].

Extensive studies have been made on the production and application of alternative non-fossil reducing agents, such as hydrogen and biochar, in several pyrometallurgical operations including smelting processes.

Hydrogen has great potential for utilization in the steel industry since it possesses certain beneficial properties including high calorific value, good thermal conductivity, high reaction rate, etc. In addition, CO_2 neutral biobased carbon provides faster reaction kinetics than fossil carbon. Although the feasibility has been shown of employing hydrogen and biobased carbon in several applications including metallurgy, and the advantage they provide in terms of CO_2 reduction, other challenges exist from a clean energy and safety perspective [9, 10, 11].

1.1 Objectives of the thesis

In the thesis work, several reductants are employed as alternative reducing agents in ironmaking and slag treatment for metal recovery and to decrease CO_2 emissions to the environment. An investigation is carried out to determine the technical feasibility of utilizing the non-metallic fraction of printed circuit boards (PCBs) in ironmaking, hydrogen in the pyrometallurgical treatment of leach residue from zinc processing, as well as various biochars in the treatment of nickel and copper smelting slags. In each study, thermodynamic calculations to simulate experiments and the application in industry are performed and compared with the results from the experiments. The objectives of the thesis were as follows:

1. Determine the effect of time and temperature on the behavior of alternative reductants by conducting lab-scale experiments.
2. Study the reaction kinetics of the reduction process and the distribution of different elements between the slag and metal phase,
3. Determine the extent of recovery of valuable elements from waste material with alternative reductants.
4. Predict the feasibility in industrial applications by performing thermodynamic modeling and comparing with the experimental results.

1.2 New scientific contribution

This thesis contributes novel scientific knowledge on the use of PCB leach residue as reductant in ironmaking. Several authors have previously investigated the recovery of valuable metals from PCB using physical, hydrometallurgical, or pyrometallurgical techniques. This study utilized the non-metallic fraction of PCB, after leaching out the metallic component, as reductant for ironmaking. In addition, hydrogen has been used as non-fossil reductant in the thermal treatment of leach residue from zinc processing. The reaction kinetics were found to be faster than earlier studies using a different reductant. The distribution of different elements during the reduction stage is presented in this thesis. Furthermore, different biochars have been used as reductant in the pyrometallurgical reduction of nickel and copper smelting slags. The kinetics of the reduction reaction for different biochars as well as the metal to slag distribution of different element have been reported. For all the reduction studies, thermodynamic calculations were carried out to forecast their application in industry.

1.3 Practical applications

The metallurgical industry faces the challenge of high emissions of greenhouse gasses and the depletion of primary resources. To curb this issue, it is crucial to utilize non-fossil fuels and reductants as well as secondary resources. In primary metal production such as ironmaking, applying non-fossil reductants minimizes the impact on the environment. This thesis investigates the feasibility of including non-fossil fuels and reductants in metallurgical processes to recover valuable metals from secondary sources like slag. Waste from discarded electronic devices has been utilized as a raw material for the reduction of iron oxide.

1.4 Outline of the thesis

This thesis consists of a compendium and four journal articles published in peer reviewed scientific journals [I-IV]. These publications are appended to the compendium. The topic is introduced briefly in the first chapter, and the second chapter gives the background of the various non-fossil reductants used in the study. Chapter 3 provides a detailed explanation of how the experiments and analyses were conducted and, in Chapter 4, the main results and their discussion are presented. The final chapter outlines the conclusions from this research.

2. Background

The chapter gives a background to the studies performed in this thesis. Previous studies on the recovery of valuable elements from secondary sources as well as the application of non-fossil reductant have been reviewed and presented in this chapter. The advantages as well as the drawbacks of employing these reductants have also been shown in chapter 2.

2.1 Recycling secondary resources

As technology and businesses are growing quickly, the use of resources and disposal of end-of-life or slightly used products are on the rise. The demand for metals worldwide is increasing and is expected to continue as a result of rapid global industrialization. This has resulted in the generation of a large amount of waste. The increasing need for raw materials along with the challenge of disposal of waste have resulted in the reuse or recycling of secondary resources. Moreover, it is reported that, in the metallurgical industry, only about 25% of mineral resources that are mined are utilized as the final product, while the remaining 75% are considered to be industrial waste [12]. Secondary resources are supplies obtained from sources such as processing waste, end-of-life products, and manufacturing waste. Some examples include electronic waste, plastics, glass, etc. The reuse and recycling of these alternative resources have received substantial attention recently due to the shortage of resources and the increasing cost of raw materials. Recycling from secondary sources could potentially decrease the overdependence on primary materials, particularly as there is growing uncertainty around the supply of primary resources. As opposed to the linear economy where products are obtained from primary sources and discarded after use, the circular economy enhances the efficiency of the use of resources by closing the product lifecycle loop through the reuse and recycling of products [13].

During the pyrometallurgical processing of metals such as copper and nickel, a large amount of slag is produced. The slag usually contains some valuable elements such as iron, copper, cobalt, and nickel, and these valuable elements can exist in the form of sulfides, oxides, or free elements. Globally, approximately 68.7 Mt of copper slag was produced in 2015 as a byproduct during the pyrometallurgical production of copper and this is expected to increase to about 100 Mt by 2050 [14, 15]. It is reported that, during the pyrometallurgical production of nickel, 6–16 tonnes of slag is generated per tonne of nickel produced [16, 17]. Moreover, large quantities of iron residue are produced during hydrometallurgical zinc processing. It is estimated that about 6.4 Mt of zinc leach residue is produced per annum and this amount is projected to increase due to the growing demand for zinc [18].

Metals can be recycled indefinitely in theory, but the complexity of the designs and functions of consumer products make recycling challenging. While these waste streams are commonly used for road construction, making cement or fertilizers, some of them are disposed of at landfill sites. From an economic point of view and to meet stringent environmental regulations, it is important to recover valuable elements from these wastes properly to ensure efficient use of resources and environmental sustainability.

The compositions of slags and zinc leach residue are heterogenous and chemically diverse, owing to the type of raw materials and the processing technique [19]. Slags contain silica and iron oxide and small amounts of aluminum, calcium, and magnesium as well as metals such as copper, nickel, and cobalt [20, 21]. Zinc leach residue consists of iron, sulfate, and zinc ferrite in addition to different impurities such as Zn, Pb, Cu, Ag, and Au [22].

Several techniques for extracting and recovering valuable elements have been studied. They can be classified as physical or chemical methods or a combination of both [19, 23]. Physical separation methods include flotation and magnetic separation [24, 25], whereas chemical separation methods comprise leaching, roasting, and reduction [18, 26, 27, 28]. Some studies have combined reduction and magnetic separation [29, 30] , roasting followed by flotation [31], as well as oxidative roasting followed by magnetic separation [19, 32]. For example, high temperature processing of zinc leach residue is currently applied at the Korea Zinc facility in Onsan, South Korea [22, 33].

The effective handling of industrial waste and secondary resources in the metallurgical industry will continue to be crucial for both environmental sustainability and economic viability, given the present circumstances.

2.2 Hydrogen as reductant

As the world transitions to non-fossil reductants and fuels, one of the most promising clean energies in the 21st century is hydrogen, since it possesses high calorific value, good thermal conductivity, and a high reaction rate among other benefits [10]. Studies done on the production [34, 35, 36] and use of hydrogen reveal the feasibility of applying hydrogen as a reducing agent for various oxides including nickel oxide, tungsten oxide, and iron oxide [37, 38, 39]. Hydrogen is reported to have a faster reaction rate compared to other reducing agents [40, 41]. Ma *et al.* studied the impact of employing hydrogen as reductant in ironmaking and stated that, although there are some economic and technology drawbacks, using hydrogen is beneficial to the environment [42]. The effects of different parameters, including temperature, H_2/CO ratio, and porosity, on the kinetics of iron ore reduction were investigated by Heidari *et al.* They reported that, while the rate of reduction increases exponentially with temperature, at temperatures above 590 °C only the reduction from Fe_2O_3 to Fe_3O_4 is affected significantly [37]. In the paper by Dang *et al.,* the authors formulated a novel kinetic model for the hydrogen-based reduction of metal oxides under isothermal and non-isothermal conditions. They reported that curves that are estimated by the model are comparable to experimental findings in the literature [43]. Luidold and Antrekowitsch stated that hydrogen can be utilized as reductant in the making of tungsten and molybdenum powders and is essential in the production of advanced materials like nanocomposites [39].

The steelmaker SSAB has formed a joint venture, HYBRIT, with LKAB (the largest iron ore producer in Europe) and Vattenfall (Swedish energy company active in many European countries), where hydrogen is applied as the reducing agent in steelmaking to produce fossil-free

steel. This technology is currently in the pilot phase and SSAB aims to bring fossil-free steel to the market by 2026 and largely eliminate carbon dioxide emissions from their operations by 2030 [44].

While producing hydrogen-based direct reduced iron is advantageous for the environment and the most advanced technique, the process of generating hydrogen is costly [45]. In addition, the method of production and the energy used to produce it has to be taken into account. Hydrogen is considered as CO_2 neutral only if the source of production is CO_2 neutral [11, 34]. According to Liu *et al.* [10] hydrogen is generally produced from fossil fuels (coal, oil, natural gas) and renewable sources (water and biomass). The technologies for hydrogen production include coke oven gas (COG) reforming, steam methane reforming (SMR), coal gasification, and the electrolysis of water. COG is the main byproduct in coke making and it consists primarily of H_2, CH_4, and CO_2. Raw COG derived directly from coke ovens is treated since it contains impurities such as naphthalene, tar, benzene, among others. Hydrogen is produced from COG when combined with CCS technology [10].

During the SMR process, the methane in the purified natural gas is reacted with steam at high temperatures to produce carbon dioxide and hydrogen according to Equation (1) [36] :

$$CH_4 + 2H_2O \rightarrow CO_2 + 4H_2 \quad (1)$$

In hydrogen production using coal gasification, coal is partially oxidized with steam and oxygen at temperatures between 800 °C and 1300 °C and a pressure of 30-70 bar to obtain CO mixed with syngas and steam. The syngas subsequently undergoes a water gas shift reaction (see ((2)), converting CO into H_2 through reaction with H_2O and the final gas is purified [36, 46, 47].

$$CO + H_2O \rightarrow CO_2 + H_2 \quad (2)$$

Another method for hydrogen production is water electrolysis, where water is split into hydrogen and oxygen using electricity with appropriate electrolysis equipment. This technique yields exceptionally pure hydrogen, i.e., a purity of 99.99%. However, the energy required and the total cost are high, which hinders the development of hydrogen production by water electrolysis [48, 49, 50].

Hydrogen can also be produced from biomass through thermochemical and biological methods. In the thermochemical method of hydrogen production, biomass is subjected to high temperatures in the absence or with a very small amount of oxygen for partial oxidation to produce hydrogen. Thermochemical processes include pyrolysis, gasification, and steam reforming of bio-oils. Biological techniques include dark fermentation, direct photolysis, photo-fermentation, and microbial electrolysis [10, 51, 52].

Hydrogen can be classified as “green hydrogen”, “gray hydrogen”, “blue hydrogen”, or “turquoise hydrogen”, depending on the production technology [53]. “Green hydrogen” is produced by the electrolysis of water using electricity derived from non-fossil sources [54]. “Gray hydrogen”, on the other hand, is produced largely via SMR and entails a substantial release of CO_2 [53, 54]. Fossil fuels are also used in the production of “blue hydrogen”; however, carbon capture and storage technologies are applied to avoid CO_2 emissions [53, 55]. “Turquoise hydrogen” is produced by the decomposition of methane. In the latter method, solid carbon is formed as a byproduct instead of CO_2 [53].

2.3 Biochar as reductant

Another reductant that can be explored to decrease CO_2 emissions is biomass (biobased carbon). As one of the main products in nature, biobased carbon has attracted a substantial amount of attention as a potential substitute due to its good combustibility and reducing ability. Biomass can be sourced from wood, crops (wheat, corn straw), etc. and is preferred because it is widely available [56]. Carbon dioxide in the atmosphere is consumed and stored up during the growth of biomass. This CO_2 returns to the environment when biomass is employed as fuel or reductant in high temperature processes. Hence the use of biomass creates a closed loop carbon cycle [57, 58]. Suopajärvi *et al.* found that incorporating biobased reductants in the blast furnace significantly decreases CO_2 emissions in steelmaking [59], while Mousa *et al.* highlighted that utilizing biomass as reductant and energy source provides a potential solution for environmentally friendly steel production [60].

Owing to some properties like high moisture content, low carbon content, and low calorific value, unprocessed biomass cannot be utilized directly as a replacement for fossil fuels. However, through processes such as pyrolysis, untreated biomass is converted to biochar or biocoke, which is an ideal substitute for conventional fossil reducing agents [56, 61, 62].

Extensive studies have been performed on the use of biochar or biobased carbon as reductant in ferrous and non-ferrous metal production. Zuo *et al.* used biochar obtained from carbonized wood as the reducing agent for hematite and compared the results to reduction by coal and coke. The results demonstrated that biochar has a higher reactivity and reduction takes place at lower temperatures in comparison to coke and coal [63]. Adrados *et al.* conducted a comparative study on biocoke derived from the pyrolysis of olives and eucalyptus in contrast to conventional reductants (metallurgical coke, petroleum coke, and anthracite). Based on proximate and ultimate analyses, their findings revealed that the biocokes exhibited better quality compared to the commercial reducing agents due to their lower ash and sulfur content. Additionally, biocokes possess significantly higher specific surface area and porosity, which renders them more reactive than commercial reductants [57].

The effect of varying temperature on the carbothermic reduction of laterite was investigated by Hidayanti *et al.* between 700 °C and 1000 °C using palm kernel shells as reductant. After the reduction experiments, they analyzed the products by XRD and found that at 800 °C and after 60 minutes, the conversion of oxide to nickel was optimal [64]. In the study by Zhou *et al.,* pyrolyzed walnut shells were employed as reductant for iron recovery from waste copper slag. Characterization of the walnut biochar revealed that it had a high fixed carbon and low sulfur content. The study showed that biochar can efficiently reduce the iron phase in the slag. Their findings were that iron recovery of 95.56% was obtained at 1300 °C, which indicates that biochar can applied as an alternative carbonaceous reductant [14]. Avarmaa *et al.* employed a mixture of biochar and battery scrap as reductant for nickel slag and compared the results to reduction with coke. The results demonstrated that, compared to coke, biochar increased the reaction kinetics [65].

Since biochar has a relatively higher volatile matter content, which contributes to reduction reactions, Bagatini *et al.* explored the reduction of iron oxide with biomass volatiles from 200 °C to 1000 °C to understand the mechanism and its application in the ironmaking industry. The authors found that, at lower temperatures (<800 °C), reduction of iron oxide occurred,

and the extent of reduction increased to 1000 °C since XRD detected FeO, Fe, and Fe_3C (cementite). In addition, it was observed that, at low temperatures, reduction took place by non-condensable gasses (CO, H_2) from biomass pyrolysis and carbon was deposited on the oxide. However, reduction progressed using the carbon deposited on the iron ore at high temperatures [66].

2.4 PCB leach residue as reductant

Electronic equipment such as computers, mobile phones, and other devices are ubiquitous nowadays owing to the advancement of technology. The lifespan of electronic products has become shorter due to frequent replacement and fewer options for repair [67]. These products are being discarded at an increasing rate, which leads to growing total amounts of electronic waste (e-waste). The total amount of e-waste generated worldwide in 2019 was 53.6 million tonnes (Mt) [68] and this amount is expected to increase annually by approximately 3-5% [69, 70]. Indiscriminate handling and improper disposal of e-waste is consequently detrimental both to humans and the environment. In 2019, it was reported that only 17.4% of the e-waste generated was collected and recycled, indicating that the rate of recycling is far behind the generation of this waste stream [71]. Electronic waste contains several parts, but the principal component is the printed circuit board (PCB). PCBs are present in almost all electronic equipment and contain many valuable components and hazardous substances [72]. Typically, the structure of a PCB is copper-clad laminate consisting of glass-reinforced epoxy resin and several metallic materials including base and precious metals [73]. From the economic and environmental points of view, recycling e-waste and metal recovery has attractive potential. It has been reported that the content of base and precious metals in PCBs is higher than in their respective ores and the gold content in PCBs is 35-50 times more than that in gold ore [74]. Additionally, based on their study of the economic potential of waste PCBs, D'Adamo *et al.* [75] suggested that metal recovery is sustainable and the net present value of PCBs ranges from 39.2 to 90.6 million euros.

Several technologies for metal recovery and PCB recycling exist and can be classified generally under physical, thermal, and chemical processing. In physical recycling, waste PCBs are shredded and crushed and the metallic fraction (MF) as well as the non-metallic fractions (NMF) are separated depending on their densities, magnetic properties, and electric conductivities [76]. High-temperature processes such as conflagrating, smelting in furnaces, sintering, and drossing can be applied for metal recovery [77, 78]. Some metal manufacturing companies like Noranda (Quebec, Canada) and Boliden Rönnskär (Sweden) apply thermal processes to recover valuable metals from electronic waste [70] .

Waste PCB is treated by hydrometallurgical techniques in chemical recycling. This process route is based on leaching, purification, and metal recovery. Targeted metals are leached using a suitable lixiviant such as sulfuric acid, cyanide, thiosulfate, or halides [74, 79]. On the one hand, this process has been found to be accurate, highly predictable, and easily controlled but on the other hand, this method does not take into account the NMF of PCBs [80] .

From a zero-waste point of view, both the MF and NMF of PCBs must be recycled to derive value in addition to reducing the impact on the environment. Some studies have recycled NMF PCB by using it as inclusions or fillers in concrete, asphalt materials, or thermoplastic resin with minimal processing while others have employed processes like pyrolysis, supercritical

fluid depolymerization, or hydrogenolytic degradation to produce chemicals and fuels from NMF PCB.

The composition of NMF PCB is complex and it contains diverse plastics and ceramics. Due to the presence of plastics, NMF PCB can be applied as a reducing agent in pyrometallurgical operations. The application of plastics- and polymer-containing materials as a replacement for coal, coke, or oil for reductive smelting has been extensively studied [81, 82, 83, 84]. This technology was first implemented by NKK Keihnn Works in Japan after development by the Bremen Steelworks in Germany [85]. Lotfian *et al.* [86] investigated the potential of substituting coal with plastics-containing shredder material by studying its devolatilization characteristics. They showed that the evolved gas is composed of H_2, CO_2, and hydrocarbons which are known to contribute to reduction reactions. Dankwah *et al.* [87] used mixed plastics as a reducing agent for reagent grade iron oxide and compared the extent of reduction to metallurgical coke under the same experimental conditions. They found that plastics reduced iron oxide to iron and concluded that mixed plastic waste can be employed as reductant in ironmaking. Wang *et al.* [88] proposed an integrated flowsheet where waste plastics mixed with coal are pulverized and heat treated at low temperatures and subsequently utilized as a reducing agent. Their study revealed that the pulverized, heated mixture showed higher reactivity and bigger metallization degree than the original coal.

2.5 Challenges and drawbacks of alternative reductants

Although alternative reductants like biocarbon are crucial to decrease CO_2 emissions into the environment, they present challenges that need to be considered before their application in metallurgical processes. In order to use these reductants on a large scale, the issue of a stable and continual supply of biobased carbon and PCB feedstock needs to be addressed [11]. Multiple biocarbon sources as well as sustainable biomass production could be explored to meet this challenge. Innovative ways of collecting discarded e-waste should also be implemented.

While extensive studies conducted on the utilization of alternative reductants show their feasibility, the technology and infrastructure needed to adopt this on a larger scale may be a challenge. More research should be done to study ways to apply these reductants on a large scale to solve this challenge [89].

Another challenge is related to the economic viability of the production and implementation of these reductants. The cost of green hydrogen especially is more expensive than other conventional reductants. Even though the cost of utilizing hydrogen and other reductants cannot compete with conventional reductants, the implementation of government policies like a carbon tax can decrease this disadvantage [36, 59].

Some drawbacks related to the low carbon content, presence of oxygen, low energy content, high moisture content, and poor grindability of biomass can be mitigated by the briquetting and pyrolysis of biomass to enable its adoption in industry [90].

3. Experimental Section

This chapter provides a detailed description of the experimental materials, apparatus, procedures, and the methods used for analysis. With the exception of Publication I, all the experiments were carried out in a vertical furnace for a specific time and rapidly quenched in ice water prior to analysis. In Publication I, reduction experiments took place in a differential scanning calorimeter and thermogravimetric (DSC TGA) instrument. Thermodynamic calculations to simulate experimental conditions were performed with FactSage™ and the results were compared to those from the experiments.

3.1 Materials and their characterization

3.1.1 PCB leach residue

Waste printed circuit boards obtained from discarded computers were manually disassembled and subsequently submerged in nitric acid (2 mol/dm^{-3}) to completely remove the soldered components. The desoldered boards were cut into sizes of about 2 cm by 2 cm with a band saw and crushed to size passing through a 2 mm sieve. The crushed PCBs underwent two stages of leaching to completely remove the metallic components. In the first step, sulfuric acid (15 wt% H_2SO_4)(purity 98%) leaching was carried out for 24 hours with a solid to liquid ratio of 100 g/L at ambient temperature. The air-dried residue was further leached with aqua regia (HCl, 32% and HNO_3, 65%) in a volumetric ratio of 3:1 to completely remove the metallic fraction. The chemicals used for leaching were supplied by United Scientific (Pty), South Africa.

The proximate and ultimate analyses of the leach residue were characterized using a LECO CS 230 and Vario EL Cube Elemental Analyzer from Elementar, respectively (see Table 1) . The ash analysis is shown in Table 2. Analysis of the leach residue was conducted at UIS Analytical Services, South Africa.

Table 1. Proximate and ultimate analyses of PCB leach residue (wt%).

Proximate Analysis	**Moisture**	**Volatile matter**	**Fixed carbon**	**Ash content**	
	3.60	44.80	11.50	40.10	
Ultimate Analysis	**C**	**H**	**N**	**S**	**O**
	30.43	3.10	1.42	0.63	20.72

Table 2. Ash content and XRF analysis of PCB leach residue (wt%).

Ash content, wt%	**SiO_2**	**Al_2O_3**	**CaO**	**Fe_2O_3**	**TiO**	**MgO**	**K_2O**	**Ba**
	84.00	6.28	6.00	0.73	0.74	0.70	0.07	0.49

3.1.2 Iron residue from zinc processing

Leach residue from zinc hydrometallurgical processing was provided by Boliden Kokkola. The residue was air-dried at 80 °C for 24 hours in a Memmert GmbH + Co. KG furnace. Pretreatment of the dried residue was carried out at 700 °C for 1 hour using 65 mL/min air flow. Several batches were pretreated and mixed to ensure homogeneity. To lower the sulfur content to less than 1 wt%, oxidation was carried out prior to reduction. Samples obtained after pretreatment and oxidation were analyzed by inductively coupled plasma optical emission spectroscopy (ICP-OES). Silica sand (Sigma Aldrich, 274739) was added to adjust the Fe/SiO_2 ratio to 1.86 (w/w). This was done to lower the melting point of the residue and to enhance the distribution of valuable elements to the alloy/speiss phase during the reduction stage [91].

Table 3. Chemical composition of iron residue after pretreatment and after oxidation at 1200 °C obtained from ICP-OES, wt%.

Element	Al	As	Bi	Ca	Fe	K	Mg	Mn	Na
Pretreated iron residue	1.4	1.4	0.023	8.0	28.8	0.33	0.07	0.04	2.5
After oxidative smelting	0.77	1.3	0.024	7.2	32.5	0.25	2.3	0.04	1.8

Element	Pb	S	Sb	Se	Si	Zn
Pretreated iron residue	4.7	14.0	0.11	0.0028	3.4	1.4
After oxidative smelting	4.9	0.46	0.12	<0.001	9.8	1.4

3.1.3 Biochar

The biochar used in the study was obtained from the University of Oulu, Finland. In Publications III and IV, four different kinds of reductants were studied in the experiments, i.e., black pellets pyrolyzed at 600 °C (B600) and 1200 °C (B1200), as well as hydrolysis lignin pyrolyzed at 600 °C (L600) and 1200 °C (L1200). Pyrolysis was conducted in a Nabertherm HT08/18 chamber furnace (Nabertherm GmbH, Lilienthal, Germany) by heating from room temperature to the final temperature at 5 °C/min heating rate using nitrogen as inert gas. Once the target temperature was reached, the samples were held there for 8 h [90]. Table 4 shows the ultimate and proximate analyses of the reductants and the ash composition analyses are shown in Table 5.

Table 4. Proximate and ultimate analyses of biochar, wt%.

		B600	B1200	L600	L1200
Ultimate Analysis	C	76.62	81.21	87.90	96.73
	H	1.56	0.00	1.73	0.07
	N	7.33	5.73	8.50	2.15
	O	0.47	0.12	0.97	0.13
	S	0.00	0.00	0.00	0.00
Proximate Analysis	Volatile matter	10.82	3.57	6.39	1.31
	Ash content	12.32	12.83	1.29	0.92
	Fixed Carbon	76.16	83.19	91.62	97.54

Table 5. Ash analysis of biochar used for the reduction study, mg/kg.

Element	Ca	Mg	Na	K	P	S	Fe	Al	Si	Mn	Ba	Cr	Cu	Ni	Zn
Lignin	290	51.0	<10	130	74	1100	810	14	<10	41	4.8	15	<1.0	12	12
Black pellet	13900	960	210	2600	560	-	680	680	7400	400	200	81	6	36	140

3.1.4 Nickel and copper slag

The industrial (i.e., ground) nickel and copper smelting slag used in Publications III and IV, respectively, were provided by Boliden Harjavalta Oy (Harjavalta, Finland). XRF (X-ray fluorescence) as well as magnetite content analyses (Satmagan) for the slag were conducted at Boliden Harjavalta Oy, see Table 6. The XRD pattern for the slags reveals that the main phases detected are fayalite (Fe_2SiO_4) and magnetite (Fe_3O_4), as shown in Figure 1.

Table 6. Compositions of Ni and Cu flash smelting furnace slags by XRF and magnetite content.

Element	Fe	Ni	Cu	Co	Cr	Zn	S	MgO	SiO_2	Al_2O_3	CaO	Pb	Fe_3O_4
Ni slag	37	3.62	0.77	0.42	0.08	0.08	0.11	7.6	33.7	2.1	1.74	-	22
Cu slag	39.47	0.08	0.67	0.06	0.04	1.91	0.55	0.42	30.72	5.07	1.41	0.18	10

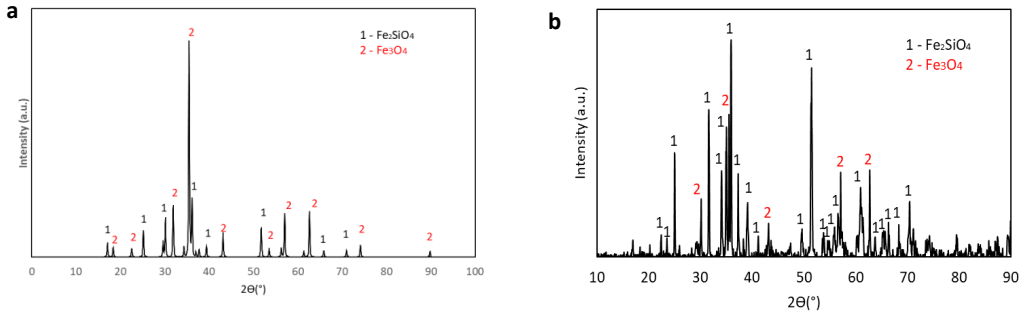

Figure 1. XRD pattern of (a) nickel and (b) copper smelting slag before reduction. This figure is reproduced from Publication III and IV, © 2023 and © 2024 Journal of Sustainable Metallurgy.

3.2 Apparatus and methods

In Publication I, hematite reduction was carried out using a differential scanning calorimeter and thermogravimetric instrument (DSC-TGA) (Netzsch STA 449 F1 Jupiter DSC-TGA with a sensitivity of ±1 µg). The DSC-TGA was connected to a Pfeiffer Vacuum ThermoStar GSD 301 T3 quadruple mass spectrometer (QMS) to qualitatively determine the species in the offgas simultaneously. In the preparation of the sample, 1 g of high purity (>99%) hematite was mixed with 0.532 g of the reductant (blends of PCB and 99.99% graphite). In each reduction experiment, approximately 20 mg of a mixture of hematite and PCB-graphite blend was weighed in an alumina crucible. The crucible was subsequently placed in the DSC-TGA and samples were heated to 1200 °C at a rate of 10 °C/min. An amount of 70 ml/min of high purity argon (99.999%) was constantly blown in the instrument to ensure an inert atmosphere. The offgas was analyzed by QMS to detect the presence of CO, CO2, and other gasses.

Figure 2 shows the schematic of the furnace that was used in Publications II, III, and IV. The vertical-tube furnace used was Lenton LTF 16/450 (Lenton Furnaces & Ovens, Hope Valley, UK) equipped with silicon carbide heating elements, placed around an alumina work tube (38 mm inner diameter and 1200 mm length) (Frialit AL23, Friatec AG, Mannheim, Germany). The temperature was monitored using an S-type Pt/Pt-10%Rh thermocouple (Johnson-Matthey Noble Metals, UK, accuracy of ±3 °C). The gas inlet and guiding tube were installed inside the work tube through a lid screw.

The furnace temperature was set to the experimental temperature and the temperature data during the experiments was collected with a NI LabVIEW temperature logging program. The thermocouple was connected to a Keithley 2010 DMM multimeter and the room temperature was measured with a Pt100 resistance thermometer (SKS-Group, Vantaa, Finland, tolerance class B 1/10), connected to a Keithley 2000 DMM multimeter. The working tube was sealed from the bottom end with a rubber plug, which had a gas outlet tube leading to an exhaust line. The furnace was equipped with water cooling elements at the top and bottom parts of the working tube. A platinum wire (diameter 0.5 mm) was inserted through the smaller diameter alumina tube for holding and lifting the samples from the cold end to the hot zone of the furnace.

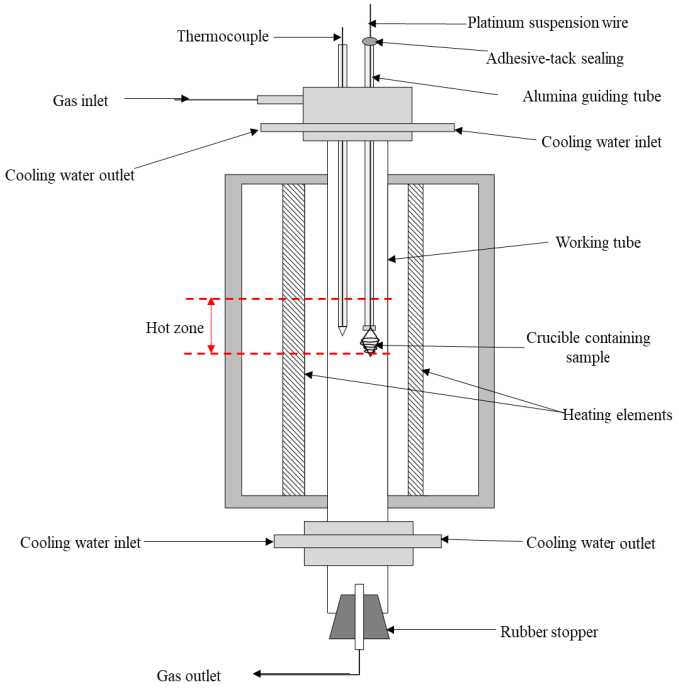

Figure 2. Schematic of the vertical furnace used for copper slag reduction experiments.

In Publication II, about 2 g of pretreated sample was placed in an MgO crucible (Tateho Ozark, Webb City, USA) and lifted into the furnace using a platinum wire which was hung from the top of the furnace. Oxidation and reduction were carried out in the furnace. During the oxidation stage, the sample was reacted with 65 mL/min oxygen (99.999 vol%) for 60 minutes [22]. The furnace was purged with nitrogen (99.999 vol%) for about 30 minutes to remove oxygen and any gas components released from the system. Afterwards, reduction was performed for 5, 10, 15, and 20 min with a mixture of hydrogen and nitrogen with 20 vol% hydrogen (99.995 vol%) and a total flow rate of 400 mL/min. Oxidation and reduction experiments were done at 1200 °C, 1250 °C, and 1300 °C. After reduction, each sample was quenched in ice water. All the gasses used in the tests were purchased from Aga-Linde Oy (Finland).

In Publications III and IV, 1 g of the slag was mixed with a calculated amount of biochar (about two times the stoichiometric amount of carbon). To estimate the stoichiometric amount, the metals content obtained from analysis of the slag was converted to the respective

oxides, as shown in Equations (3)-(7). The stoichiometric mass of carbon required was estimated from Equations (8)-(13).

$$Ni + 0.5O_2 \rightarrow NiO \quad (3)$$
$$2Cu + 0.5O_2 \rightarrow Cu_2O \quad (4)$$
$$Co + 0.5O_2 \rightarrow CoO \quad (5)$$
$$Zn + 0.5O_2 \rightarrow ZnO \quad (6)$$
$$2Cr + 0.5O_2 \rightarrow Cr_2O_3 \quad (7)$$

$$Fe_3O_4 + C \rightarrow 3FeO + CO \quad (8)$$
$$NiO + C \rightarrow Ni + CO \quad (9)$$
$$Cu_2O + C \rightarrow 2Cu + CO \quad (10)$$
$$CoO + C \rightarrow Co + CO \quad (11)$$
$$ZnO + C \rightarrow Zn + CO \quad (12)$$
$$Cr_2O_3 + 3C \rightarrow 2Cr + 3CO \quad (13)$$

The slag and biochar were weighed and mixed using a mortar and pestle and subsequently pelletized. The pellet was placed in a silica crucible (Heraeus HSQ®300 crucible of fused quartz with a purity of >99.998 wt% by Finnish Special Glass Oy, Espoo, Finland, with a diameter of 25 mm and height of 15 mm), which was in a basket-shaped sample holder made from Kanthal A1 wire (diameter 0.65 mm). The basket was attached to a platinum wire hanging from the inside of the furnace and suspended in the lower end of the furnace. To create an inert atmosphere, 300 mL/min argon gas (99.999 vol% purity, Woikoski Oy, Finland) was used to purge the furnace. After about 15 min, the sample was lifted to the hot zone. The sample was dropped into ice water by pulling the platinum wire after reaching the desired reaction time.

Reduction experiments were performed at 1400 °C for 15, 30, and 60 minutes for each of the reductants in Publication III. However, in Publication IV, the experiments took place at 1250 °C, 1300 °C, and 1350 °C for 60 min to study the effect of temperature on reduction; the effect of reaction time was studied at 1250 °C for 15, 30, and 60 min for each reductant. In Publication IV, the offgasses were analyzed using a Gasmet FT-IR gas analyzer model DX4000, (Gasmet Technologies Oy, Vantaa, Finland) to measure the CO and CO2 concentrations during the experiments. The flow rates of the input gasses were controlled by rotameters and the offgas was filtered to prevent dust from entering the gas analyzer. The gas analyzer was flushed constantly with nitrogen gas at a flow rate of 1400 ml/min to obtain sufficient total gas flow rates for reliable gas analyzer operation. The additional nitrogen was introduced to the gas line after the furnace, so it did not enter the furnace and thus did not affect the reactions. The intervals in which the offgas composition was measured were 50 s long (30 s of pumping gas to the chamber followed by 20 s of gas analysis).

3.3 Analyses of sample products

At the end of the experiments, the samples were mounted in epoxy, polished, and carbon coated for analysis. In Publications III and IV, the samples were cut in half after curing and cast in epoxy again prior to polishing and coating. The coated samples were analyzed by scanning electron microscopy (SEM-EDS) and electron probe microanalysis (EPMA). Preliminary elemental analyses and microstructural imaging was conducted with a Mira 3 scanning electron microscope (Tescan, Brno, Czech Republic) equipped with an UltraDry silicon drift energy

dispersive X-ray spectrometer (EDS) supplied by Thermo Fisher Scientific (Waltham, MA, USA).

The accurate compositions of the phases formed during reduction were measured using EPMA with an SX100 (Cameca SAS, Gennevilliers, France) microprobe equipped with five wavelength dispersive spectrometers (WDS). The accelerating voltage and beam current were 20 kV and 60 nA, respectively. Defocused 2 μm or 20 μm beam diameters were used.

Standardization of the characteristic X-ray lines to be measured for the individual elements was carried out using natural and synthetic minerals as follows: Si Kα (quartz), O Kα (obsidian), Mg Kα and Ca Kα (diopside), Al Kα (almandine), Mn Kα (rhodonite), Ni Kα (pure nickel), Co Kα (cobalt), Cr Kα (chromite), Ti Kα (rutile), Fe Kα (hematite), Cu Kα (pure copper), Zn Kα (ZnS), S Kα (pentlandite), Na Kα (tugtupite), K Kα (sanidine), Ag Lα (silver), Sb Lα (SbTe), As Kβ (GaAs), Sn Lα (pure Sn metal), and Pb Mα (galena). Totals of the individual analysis points obtained with EPMA were typically within 100 ± 2%. PAP and ZAF matrix correction [92] by Cameca was used for the primary WDS data.

In Publication II, the bulk chemical compositions of the samples before and after pretreatment as well as after oxidation were analyzed by ICP-OES, with iCAP 6000 series (Thermo Fisher Scientific, USA) apparatus. The samples were prepared for analysis by microwave digestion (MARS6 microwave digestion system, CEM Corporation, USA) using a mixture of HNO3, HCl, and HBF4 as the digestion medium.

Since the concentrations of Ni, Co, and As in the slags in Publication IV were below the detection limits of EPMA, the slags were analyzed using laser ablation-inductively coupled plasma-mass spectrometry (LA-ICP-MS), comprising an ArF excimer laser (Teledyne CETAC Technologies, Omaha, USA) and a single-collector sector field ICP-MS (Nu Instruments Ltd., Wrexham, UK). The laser was fired at 10 Hz frequency with a 40 μm spot size. Eight spots were analyzed from each sample, and 40 seconds of time-resolved analysis signal was obtained from each spot. The signals were treated using Glitter software [93]. USGS GSE-1G glass was used as the external standard, and ^{29}Si (from EPMA) as the internal standard. USGS GSD-1G as well as BHVO-2G and BCR-2G glass were analyzed as unknowns [94].

Table 7 . Average detection limits for the metal and slag from EPMA, and for slag from LA-ICP-MS analysis, ppm.

EPMA	Si	Co	Ni	As	Na	O	Al	Mg	Ca	K	S	Fe	Zn	Cu	Ti	Cr	Sb	Sn
Metal	215	300	260	4247	427	1249	288	246	78	83	107	174	354	308	212	176	382	472
EPMA	Si	Co	Ni	As	Na	O	Al	Mg	Ca	K	S	Fe	Zn	Cu	Ti	Cr	Sb	Sn
Slag	242	324	300	4925	619	580	385	224	90	95	124	203	414	409	221	189	406	540
LA-ICP-MS Slag	^{29}Si	^{59}Co	^{60}Ni	^{75}As														
	9.778	0.014	0.119	0.114														

3.4 Thermodynamic calculations

In this thesis, the FactSage™ thermodynamic software package [95] was used to investigate the effect of the addition of various reductants on the reduction products. The results from FactSage™ calculation were compared with the respective experiments. The composition of the reagent obtained from analysis was used as input in the software. The databases used for the calculations were custom collected, based on the FactPS (pure substances), FToxid (optimized for oxide systems), and FSCopp (optimized for copper-containing solid and liquid alloys) databases. The solution phases selected for the calculations were spinel (solid solution

phase with stoichiometry AB_2O_4, A, B = divalent and trivalent metals), slag (liquid oxide silicate phase), monoxide phase (solid solution), FCC, BCC, HCP-A3 (three solid multicomponent alloys), and liquid metal. Ideal gas and pure solids were also selected before the calculations were made.

In Publication IV, HSC Chemistry software was used to estimate the standard Gibbs energy for determining the sequence of reactions and the reactions that are feasible at the experimental temperatures.

4. Results and Discussion

The main findings from the experiments and thermodynamic calculations are presented and discussed in this chapter. Different non-fossil reducing agents were employed and the microstructure images and composition of the various phases obtained during the reduction reactions are shown. The experiments were conducted to investigate the effect of time and temperature as well as the addition of reductant on metal recovery and distribution of metals. The distribution coefficient of elements between metal and slag phases are shown in Publications III and IV.

4.1 Reduction of iron oxide with PCB leach residue

The ultimate analysis revealed that the PCBs contained carbon (30.43 wt%) and hydrogen (3.10 wt%), indicating that hydrocarbons existed in the PCBs. The carbon concentration is significantly lower than in coal (80.10 wt%), [96], whereas the oxygen concentration in PCBs (20.72 wt%) is far higher than that of coal (2.12 wt%). It was found that a high oxygen content led to increased CO_2 formation during reduction with PCBs. Moreover, the PCBs had an ash content of about 40.1%, which is higher than that of coal (11.7%). The high ash content is due to the presence of glass fiber and ceramics in PCBs. The glass fiber and ceramics are mainly composed of SiO_2, Al_2O_3, and CaO.

4.1.1 Thermal behavior of reagents

The reagents, hematite, graphite, and PCBs were placed separately in the DSC-TGA. No notable mass loss was seen when hematite alone or graphite alone was heated to 1200 ℃. However, a significant change was observed during the test with PCBs alone (see Figure 3). At temperatures between 275 ℃ and 325 ℃, close to 30% of the PCB mass was lost. This was because of the pyrolysis of the PCBs, where epoxy resin and flame retardants and some of the polymer content decomposed into gaseous state. Other studies on thermal treatment of PCBs also observed this change [97, 98] . The mass loss is accompanied by emission of CO, CO_2, HBr, S_2, and hydrocarbons such as CH_4 and C_2H_6 in the evolved gas.

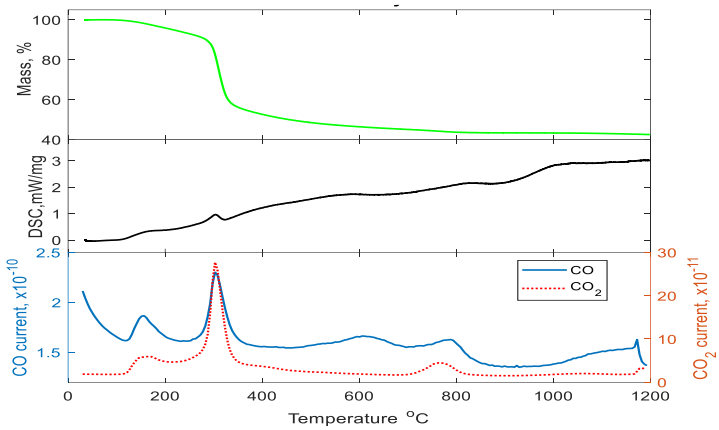

Figure 3. Mass loss, DSC, and CO, and CO_2 in offgas when PCBs are heated in DSC-TGA from room temperature to 1200 °C. This figure is reproduced from Publication I, © 2020 Minerals Engineering.

4.1.2 Hematite reduction with graphite-PCB blends

Reduction experiments performed with graphite showed that reduction started at around 900 °C, as the sample lost mass and QMS detected CO and CO_2 in the evolved gas at that temperature. In addition, it was observed that around 1120 °C, the mass of the sample plummeted with a corresponding release of CO and CO_2 and an endothermic DSC peak. This may have been due to the formation of metallic iron. Moreover, Jung and Yi [99] stated that the formation of metallic iron from FeO enhances the gasification of carbon to CO. The huge mass loss may be due to carbon gasification or the Boudouard reaction (see Equation (14). Another endothermic peak was observed at 1150 °C. This agrees with the calculated eutectic temperature of 1153 °C in the Fe-C system. Since iron oxide does not melt in the presence of carbon, the peak can be ascribed to the reaction of C with the reduced pure iron:

$$C + CO_2 \rightarrow 2CO \quad (14)$$

Figure 4 shows the mass loss, DSC, and CO-CO_2 in the evolved gas during the reduction of hematite with different blends of PCB and graphite. During hematite reduction with PCBs (see Figure 4b), the mass loss at 300 °C can be attributed to the pyrolysis of the PCBs. However, the continuous loss of mass (>500 °C) with the corresponding release of CO and CO_2 indicates that the reduction of hematite with PCBs occurs earlier than the reduction with graphite. The results suggest that the kinetics of hematite reduction is faster with PCBs than with graphite. During the hematite-PCB reduction experiment, volatiles containing hydrogen and hydrocarbons that can reduce hematite at lower temperatures were liberated. Hydrocarbons such as CH_4 and C_2H_6 were detected with the mass spectrometer. In addition, due to the high volatile matter percentage in PCBs, porosity increases, and this accelerates the mass transfer conditions in the gas-solid reaction system and increases the reaction interfacial area for reduction, which improves the reduction of iron oxide.

During hematite reduction with the PCB-graphite blend, it was observed that each experiment demonstrated the same behavior as hematite-PCB and hematite-graphite reductions. It was observed that a greater amount of PCBs in the blend decreased the endothermic peak at 1120 °C. This implies that less energy is required for iron formation. The lower endothermic

peak can also be attributed to the declining weight percentage of carbon and rising volatile content in the blend.

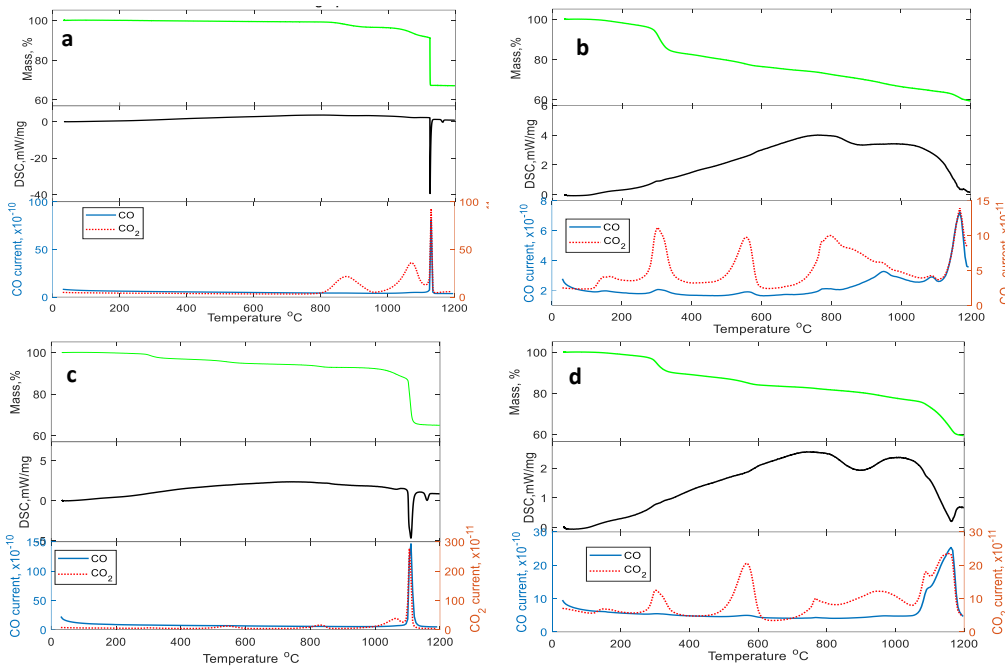

Figure 4. Mass loss, DSC, and CO and CO_2 in offgas during reduction of hematite with (a) graphite (b) PCB (c) 20% PCB and 80% PCB. This figure is reproduced from Publication I, © 2020 Minerals Engineering.

4.1.3 Degree of reduction

The degree of reduction is used to estimate how much oxygen has been removed from the hematite. It was calculated based on the mass lost during the reduction (see Equation (15)) in the DSC-TGA using Equation (16) [99]. During reduction with the PCBs and PCB blends, the mass loss that did not contribute to the reduction of hematite was taken into account when calculating the reduction degree (see Figure 5).

The overall reduction may be expressed by the reaction:

$$Fe_2O_{3\,(s)} + 3C_{(s)} \rightarrow 2Fe_{(s)} + 3CO_{(g)} \quad (15)$$

$$\text{Reduction degree} = \frac{{}^{\Delta W}/_{W}}{{}^{3MW_{CO}}/_{(MW_{Fe2O3}+3MW_C)}}, \quad (16)$$

where ΔW = mass lost; W = initial mass; MW_{CO} = molecular weight of CO; MW_{Fe2O3} = molecular weight of Fe_2O_3, and MW_C = molecular weight of C.

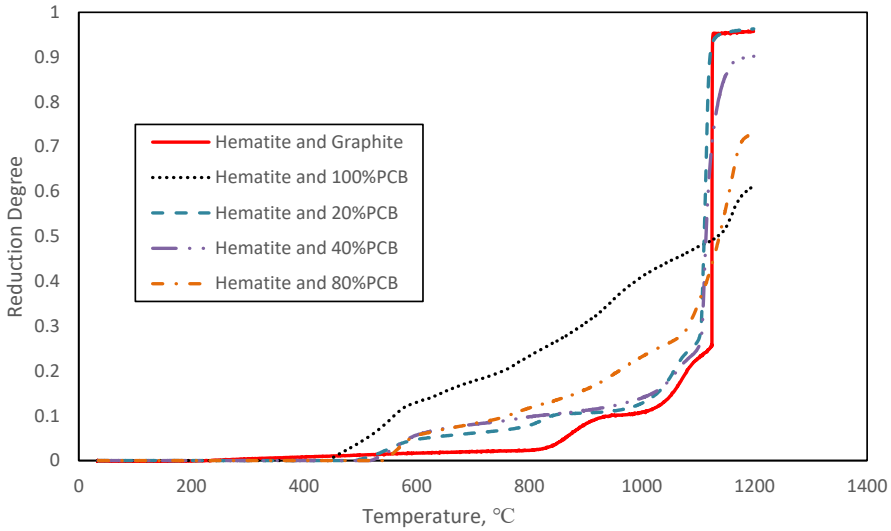

Figure 5. Reduction degree of hematite reduction with blends of graphite and PCBs. This figure is reproduced from Publication I, © 2020, Minerals Engineering.

The calculation of the degree of reduction showed that, although PCB acts as a better reductant at lower temperatures (<1000 ℃), at higher temperatures (> 1100 ℃) graphite is more beneficial. It was observed that the overall degree of reduction decreases when increasing the mass percent of PCBs in the reductant. However, the highest reduction degree (97%) was achieved when the blend of graphite and 20% PCB was employed as reducing agent.

4.1.4 Thermodynamic simulation of hematite reduction with graphite and PCB blend

FactSage™ was employed as a tool to calculate and predict the products of hematite reduction with blends of PCB and graphite in experimental conditions. The masses used in preparing each sample were used as input in FactSage™ and calculations were performed from room temperature to 1600 ℃. The results (see Figure 6) show that the formation of solid iron starts around 700 °C for all the reduction tests. Liquid iron in the alloy forms at temperatures above 1150 °C for all the reduction tests apart from the hematite-100%PCB reduction. In the lab scale experiments, a large mass loss is also observed around 1150 °C. This is because iron and carbon start to melt at this temperature which increases the kinetics of reduction reaction. When PCB or blends of PCB are used as reductants, FactSage™ predicts the formation of fayalite (Fe_2SiO_4) between temperatures 200 °C and 800 °C. This is due to the presence of SiO_2 in the PCB.

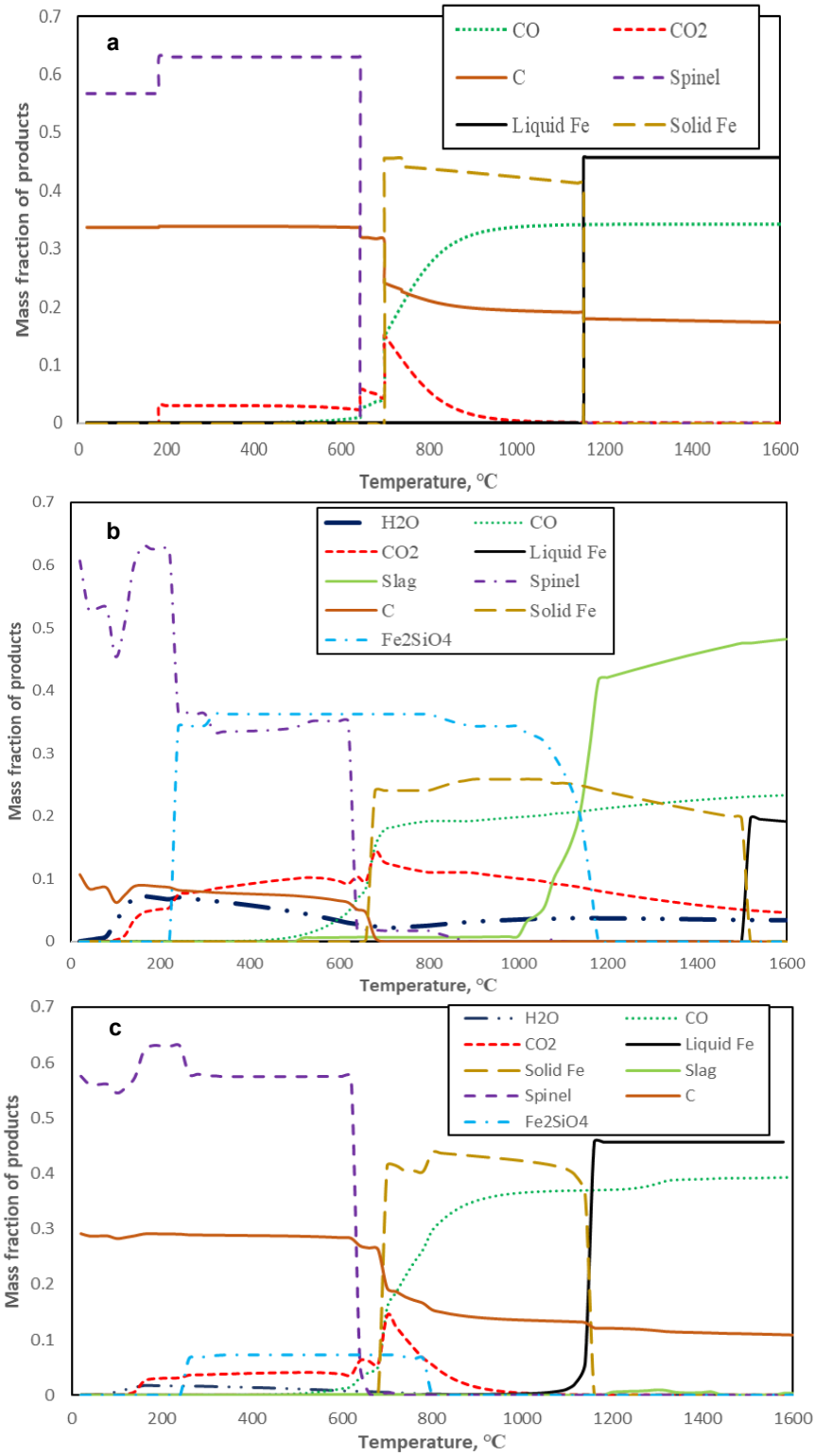

Figure 6. Mass fraction of products obtained from FactSage™ calculation during hematite reduction with a) graphite b) 100% PCB c) 20% PCB. This figure is reproduced from Publication I, © 2020 Minerals Engineering.

4.2 Reduction of zinc leach residue with hydrogen

4.2.1 Oxidation stage

Oxidation of pretreated zinc leach residue was performed prior to hydrogen reduction to convert the metals present in the residue to oxides in the slag as well as decreasing the sulfur content to less than 1 wt% [100, 101] .

As shown in the SEM images (Figure 7), two phases: molten slag and solids, are formed after oxidation at the experimental temperatures. The solids (light gray areas), predominantly iron oxide, are scattered within the molten slag (darker gray areas). The molten slag is mainly composed of oxides of Fe, Si, Ca, and Pb. The dark regions are cracks found within the samples, which is due to the thermal shock experienced during quenching.

Oxygen reacts with elemental sulfur or metal sulfide that may be present in the sample during this oxidation stage. The concentration of sulfur in the slag decreased notably at all the temperatures, which indicates that oxygen had adequate contact with the sample. Increasing the temperature resulted in an increase in the MgO concentration in the solids and slag because the reaction between the slag and the MgO crucible intensified.

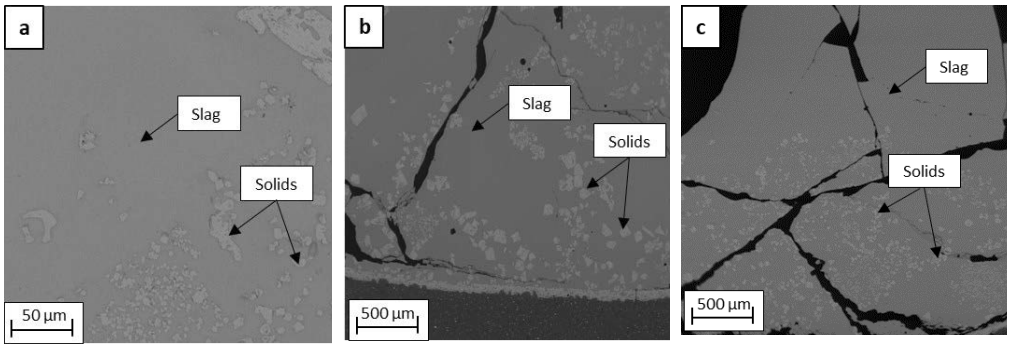

Figure 7. Micrographs of the iron residue containing molten slag and iron oxide after oxidation step at (a) 1200 ℃, (b) 1250 ℃, and (c) 1300 ℃ for one hour. This figure is reproduced from Publication II, © 2022 Metallurgical and Materials Transactions B.

4.2.2 Reduction stage

The metal oxides that were formed during the oxidation step were reduced with hydrogen in the reduction stage. The elements in the sample were distributed into the gas, slag, solid (spinel), and metal phases during reduction. Volatile metals are expected to be released into the gas phase. The metallic phase, also known as speiss, that was formed during reduction settled at the bottom of the crucible. The speiss is made of metal (typically Fe or Ni) arsenides or antimonides. In non-ferrous smelters, the speiss generated is not desirable as significant amounts of precious metals and copper are dissolved in it [102]. However, in the zinc leach residue treatment process, the formation of speiss is advantageous as it helps to gather valuable metals from the slag.

SEM images of the samples after the reduction experiments at 1300 ℃ (Figure 8) revealed that there were no metal droplets present in the sample after five minutes of blowing hydrogen. After 10 min and longer, however, small heterogenous speiss droplets with Pb-rich and As-Cu-rich areas were formed. The metal droplets formed after 10 min at all the reduction temperatures indicate that hydrogen serves as a highly effective reductant. Nurmi [100] reported that

speiss consisting of copper, antimony, and lead was formed after 120 min in their study on reduction of zinc leach residue using CO/CO_2. Similarly, Rinne [101] employed a blend of coke and biochar as reductant in pyrometallurgical treatment and observed the formation of speiss after 20 min.

While Pb was expected to evaporate during the reduction experiment, the speiss contained Pb-rich regions which generally decreased at higher temperatures. Pb is probably trapped within the slag, making it difficult for it to vaporize into the offgas. The iron oxide (Fe_3O_4) that was present in the sample after oxidation was reduced by hydrogen to FeO which dissolved in the molten slag. At elevated temperatures, the MgO crucible dissolved into the slag as reduction occurred and formed some kind of ferrous-based spinel ($(Fe,Mg)(Fe)_2O_4$) at the rim of the crucible (interface of the slag and crucible). Iron oxide was also observed at the slag and crucible interface after about 15 min.

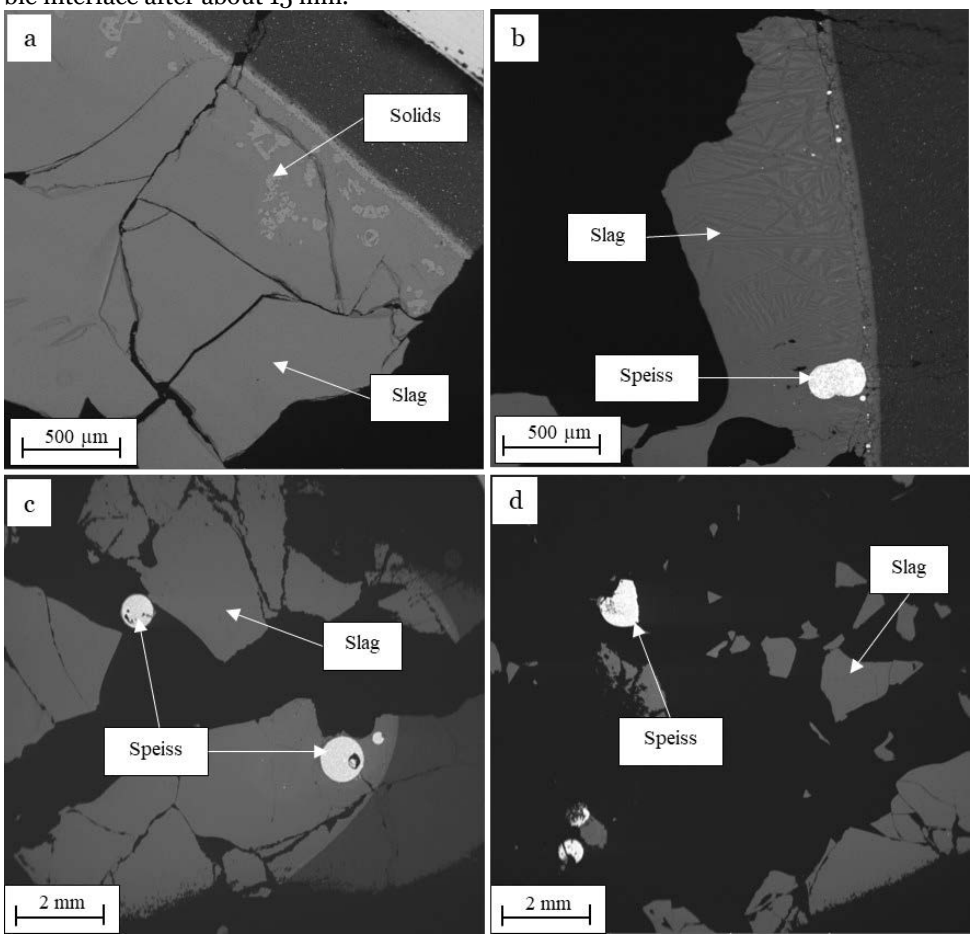

Figure 8. Micrographs of iron residue after reduction at 1300 ℃ after (a) 5, (b) 10, (c) 15, and (d) 20 minutes. This figure is reproduced from Publication II, © 2022 Metallurgical and Materials Transactions B.

Since the concentrations of Pb and other volatile metals did not decrease as expected, another set of experiments was performed at 1300 ℃, where the samples were kept in the furnace under inert conditions for one hour after conducting reductions for various lengths of time. The purpose of this was to assess whether the volatilization of certain elements increased and find out whether the smaller speiss droplets would coalesce into bigger droplets. Additionally, this was

done to determine whether the sample behavior agreed with the thermodynamic model. The analysis showed that volatile element concentrations in the slag phase were lower than in the tests without one hour under inert conditions.

The SEM image after 15 min reduction and one hour under inert conditions revealed that the speiss that was produced consisted of Fe-As regions combined with a Pb-rich area. This observation concurs with the thermodynamic simulations presented in the next section. Thermodynamic calculations with FactSage™ predict the formation of two liquid metal phases at oxygen partial pressures of less than $10^{-9.6}$ atm.

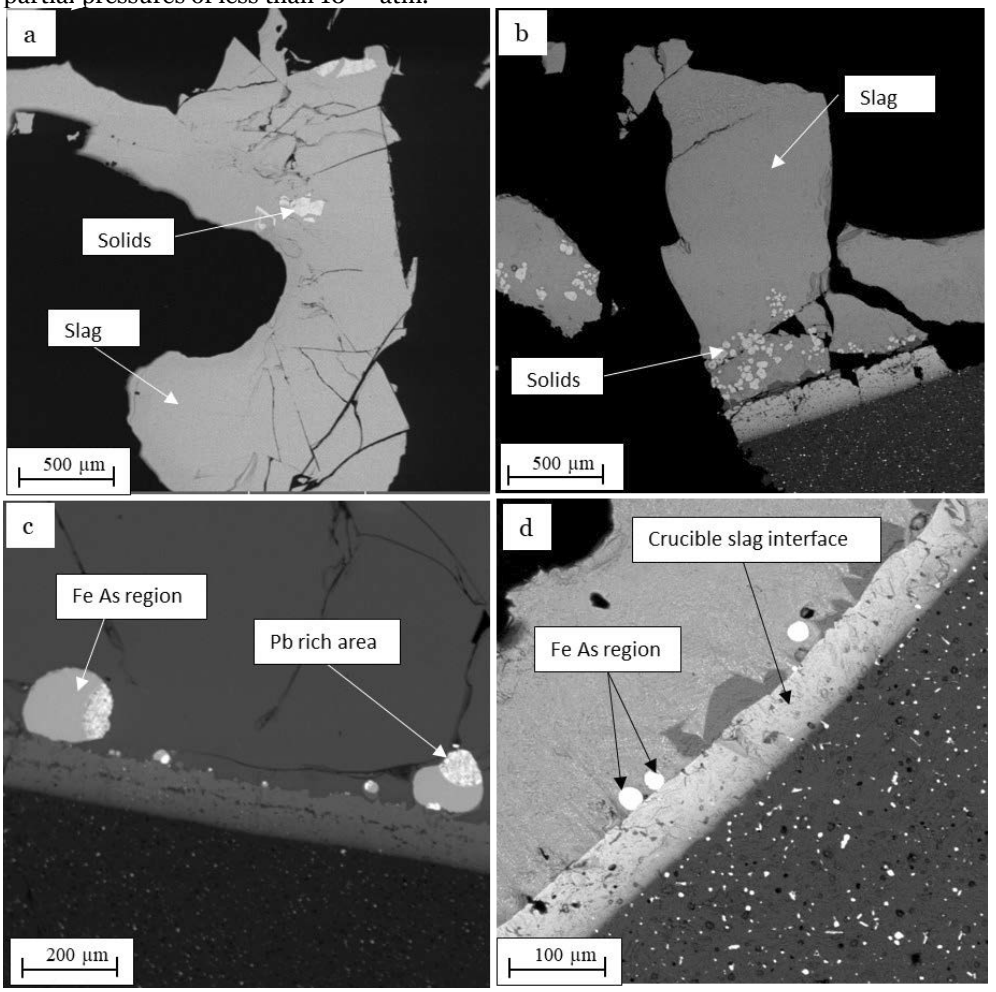

Figure 9. Micrographs of iron residue post reduction at 1300 °C after (a) 5, (b) 10, (c) 15, and (d) 20 minutes, and 1 hour under inert conditions. This figure is reproduced from Publication II, © 2022 Metallurgical and Materials Transactions B.

4.2.3 Thermodynamic simulation of zinc leach residue with hydrogen

FactSage™ was used to perform thermodynamic calculations to simulate the reaction for its industrial application and for comparison with the experimental results. Two scenarios were considered. In the first case, the oxygen partial pressure ($P(O_2)$) was varied to predict the phase equilibrium (see Figure 10). A $P(O_2)$ within the range of 10^{-5} and 10^{-12} was selected because only

the slag or slag + liquid metal is stable. However, this scenario does not fully represent the volatilization behavior of the various elements and the formation of gas phase is minimal.

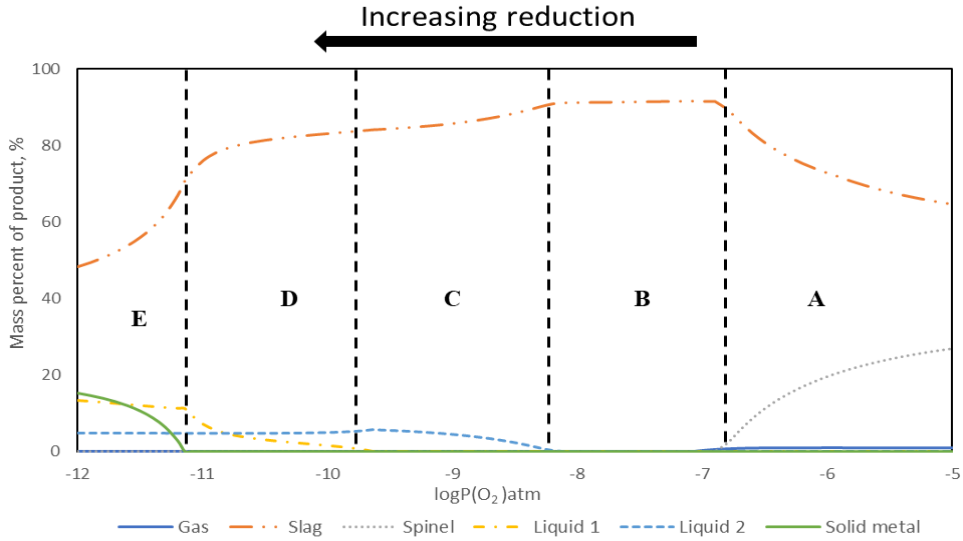

Figure 10. Mass of phases obtained from reduction at 1300 °C for $P(O_2)$ between 10^{-5} and 10^{-12} atm. This figure is reproduced from Publication II, © 2022 Metallurgical and Materials Transactions B.

As shown in Figure 10, the sample primarily consists of slag and spinel at higher oxygen partial pressure ($>10^{-6.8}$ atm). Spinel disappears and only slag is present within 10^{-7} and 10^{-8} atm as the reduction degree increases. At an oxygen partial pressure lower than 10^{-8} atm, liquid metal emerges, while a different liquid metal phase forms at less than $10^{-9.6}$ atm. A closer look at the composition of Liquid 1 indicates that it is predominantly Fe and As while Liquid 2 is over 90 wt% Pb. FactSage™ predicts that solid metal, mainly (>98%) Fe, precipitates from the slag when reduction continues up to less than a $P(O_2)$ of $10^{-11.2}$ atm.

Figure 11 illustrates the distribution of the four elements of interest (Pb, As, Zn, Cu) in the various phases. Pb deports from the slag to the liquid metal phase starting from $P(O_2) < 10^{-8}$ atm. Most of the As is in the slag phase between 10^{-8} and 10^{-6} atm $P(O_2)$. The As in the slag is continuously reduced in the liquid metal phase as the oxygen partial pressure decreases ($<10^{-8}$ atm). Due to the low pressure in the system, Zn does not vaporize to the gas phase but remains mostly in the slag phase and partly present in the liquid alloy phase at $<10^{-11}$ $P(O_2)$.

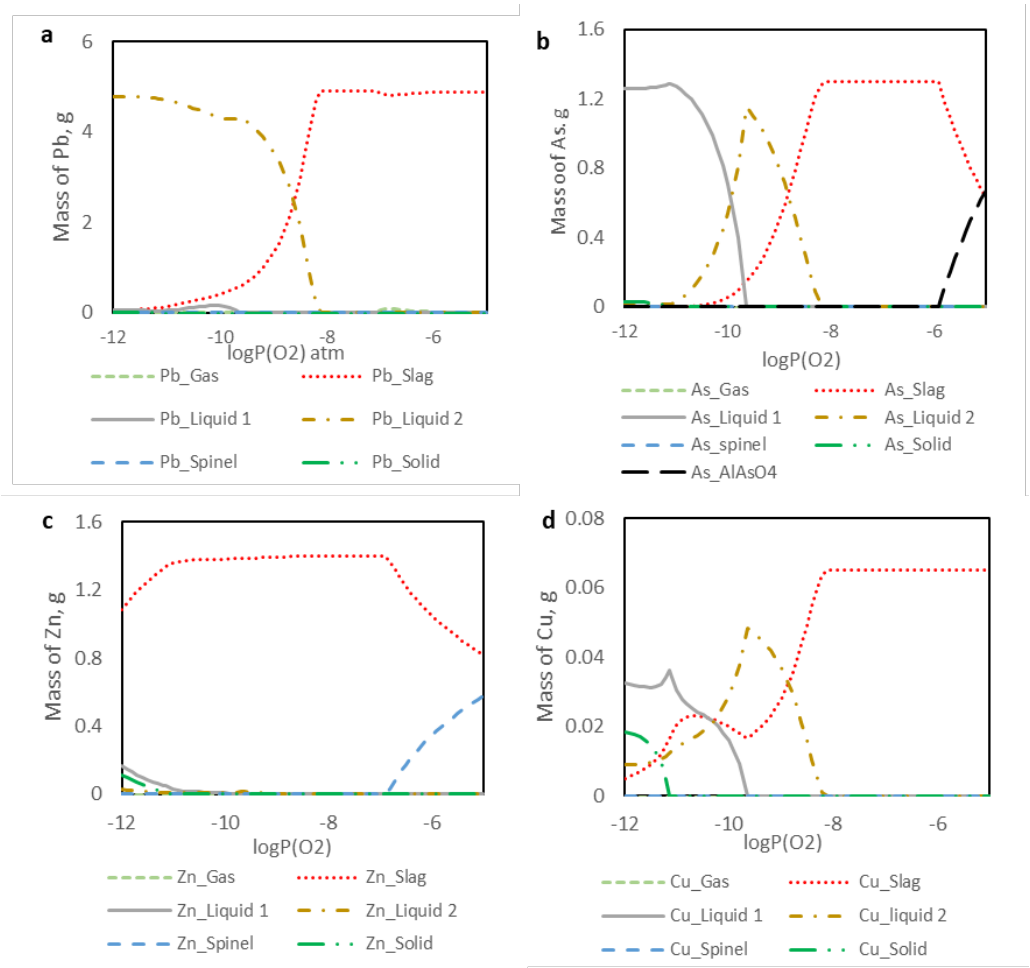

Figure 11. Elemental distribution of (a) Pb, (b) As, (c) Zn, (d) Cu obtained from reduction at 1300 °C for $P(O_2)$ between 10^{-5} and 10^{-12} atm. This figure is reproduced from Publication II, © 2022 Metallurgical and Materials Transactions B.

In the second scenario, the parameters employed during the reduction experiments at 1300 °C were utilized as input for FactSage. The open calculation feature in FactSage™ was used to simulate the reduction of impure slag (after oxidation). In this mode, gas produced in the reduction step at fixed pressure and temperature is removed and unreacted gas (mixture of H_2 and Ar) is added to the equilibrated solid and liquid phases from the previous step. This is repeated multiple times as needed. This was done to relate the calculations to an ideal case of a time-dependent experiment, assuming that all added gas is allowed to react with the condensed phases.

Figure 12 shows the total mass of the different phases produced during reduction. It can be observed that, in the first four minutes, spinel and slag are present but spinel subsequently disappears. While liquid metal of less than 0.2 wt% is formed between 7 min and 9 min, solid metal, mainly Fe, is produced after 7 min of reduction. The mass of slag steadily decreases while the solid metal increases. This indicates that the iron oxide in the slag is reduced to iron.

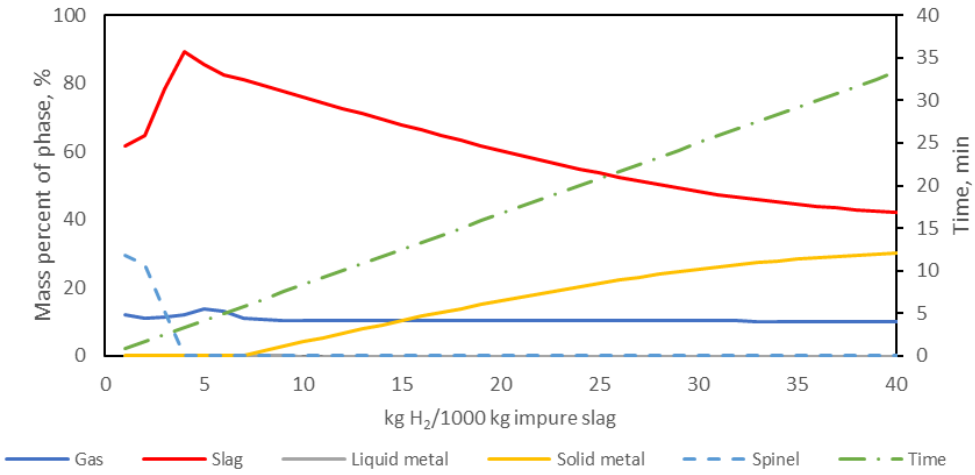

Figure 12. Mass of phases obtained from impure slag reduction at 1300 °C with 20 vol% H_2 predicted by FactSage. This figure is reproduced from Publication II, © 2022 Metallurgical and Materials Transactions B.

The distributions of some elements of interest, when hydrogen is used as reductant, are shown in Figure 13. It can be observed that Pb and As are completely released into the offgas after about 6 min. Zn is distributed between spinel and slag within the first 4 min and ultimately fumed to the gas phase from the slag phase. After 6 min of reduction, the concentration of copper in the slag begins to decrease as copper deports into the solid metal phase.

The results of this calculation support the experimental results that were observed at 1300 °C after reduction at 15 min and one hour under inert conditions. Within 6 and 8 min of reduction, close to 10% of the Cu content in the zinc residue is present in the liquid metal.

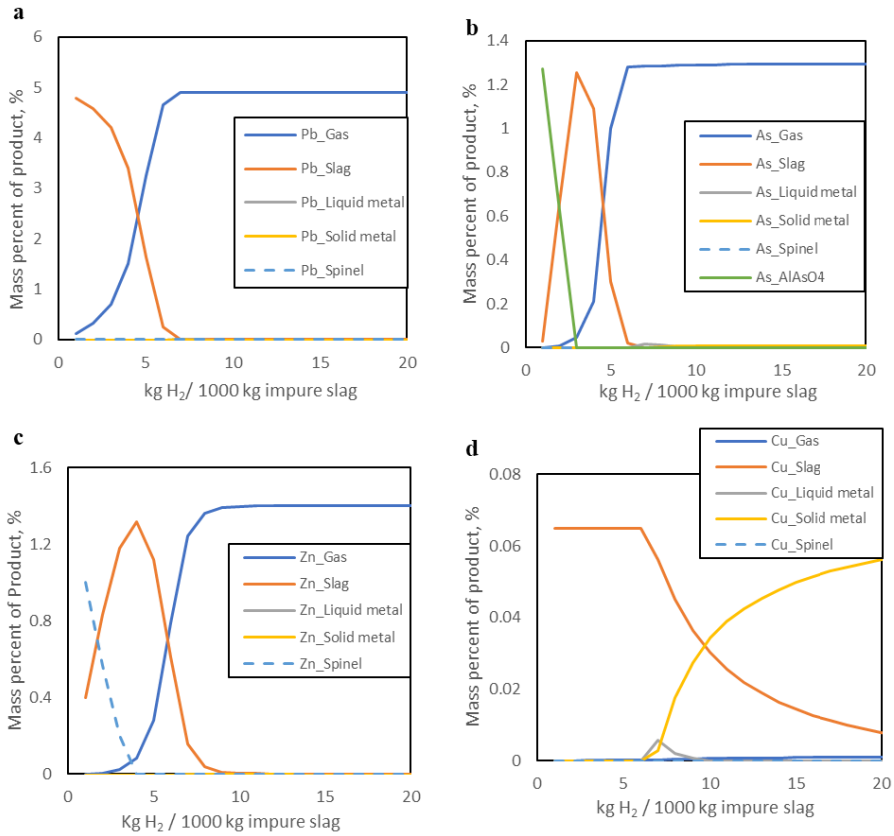

Figure 13. Elemental distributions of (a) Pb, (b) As, (c) Zn, (d) Cu obtained from impure slag reduction at 1300 °C with 20 vol% H2 after 20 min predicted by FactSage™. This figure is reproduced from Publication II, © 2022 Metallurgical and Materials Transactions B.

4.3 Nickel slag reduction with biochar

Thermal treatment of industrial nickel slag was conducted at 1400 °C in a vertical furnace as a function of reaction time. The sample melts at the reduction temperature and the metal oxides (MeO) in the slag react with carbon as well as the released CO. The concentration of metals in the slag decreases as time proceeds, while the reduced metal and mechanically entrapped droplets combine and grow to form a metal alloy.

SEM analysis showed that metal droplets (bright round regions) were produced at every reduction time, indicating that reactions proceeded rapidly. Figure 14 presents typical SEM micrographs of sample polished sections prepared from nickel slag reduction with L600 biochar at 15, 30, and 60 minutes. The slag phase (gray region) was generally homogenous.

Since the samples were quenched rapidly, some of the solidified slags were brittle, which resulted in some slag pieces as well as metal alloy breaking off from the rest of the sample when being cut. The dark regions (epoxy) present within the slag are ascribed to the aforementioned gas formation in the melt. During some of the reduction experiments, two metal alloys were observed, one larger and the other smaller. The larger one (> 1 mm diameter) is believed to be formed first and the smaller droplets formed later. Upon analyzing the smaller droplets, it was observed that they contained higher concentrations of nickel, cobalt, and copper, but a lower concentration of iron compared to the larger droplet.

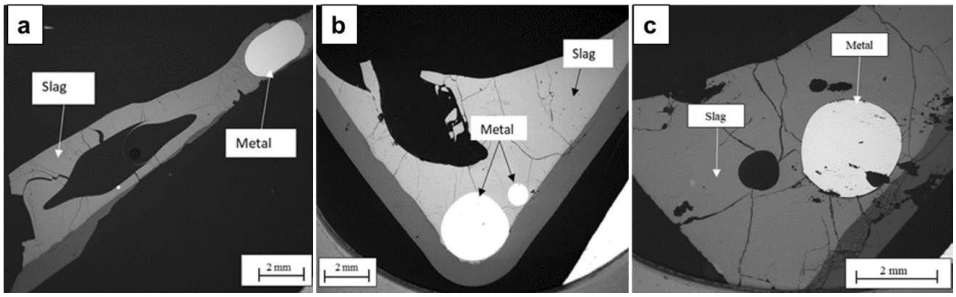

Figure 14. SEM micrographs of sample polished sections of nickel slag with L600 biochar for (a) 15, (b) 30, and (c) 60 minutes. This figure is reproduced from Publication III, © 2023 Journal of Sustainable Metallurgy.

Reduction experiments were performed with metallurgical coke (Figure 15) as reductant and the results were compared with biochar reduction experiments. The large metal alloy droplets (~2 mm diameter) found during biochar reduction were absent when coke was employed as reductant. This indicates that biochar is a more reactive reducing agent compared to metallurgical coke.

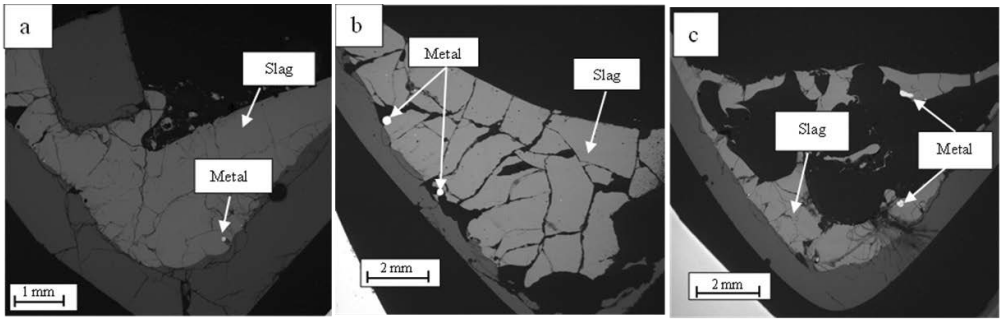

Figure 15. SEM micrographs of sample polished sections of nickel slag with coke for (a) 15, (b) 30, and (c) 60 minutes. This figure is reproduced from Publication III, © 2023 Journal of Sustainable Metallurgy.

The concentrations of selected elements: nickel, cobalt, copper, and iron, in the slag as time progressed are shown in Figure 16. This provides an estimate of the amount of different elements that evolve to the gas phase or are reduced to the metal alloy phase. The concentrations of the metals in the slag steeply decreased within the first 15 minutes and continuously with time for all the biochar types. Nickel concentrations decreased from 3.62 wt% to 1.06 wt% when metallurgical coke was employed, while nickel was removed almost completely from the slag when B600 biochar was used. It was observed that the biochars pyrolyzed at 600 °C (L600 and B600) exhibited higher reduction potentials than the biochars pyrolyzed at 1200 °C. Although the biochars pyrolyzed at 1200 °C contained higher carbon percentages, the higher volatile matter concentrations in L600 and B600 may indirectly contribute to their faster reduction. Although reduction with coke had the lowest iron concentration in the slag, the distribution coefficient of iron was not improved. This is attributed to very small concentration of Fe in the metal phase during reduction experiments with coke. Moreover, the low Fe concentration in experiments with coke may be due to a lot of the silica crucible melting into the slag during experiments.

It has been mentioned that in slag cleaning processes (at 1300-1400 °C) and, e.g., in titania smelting, volatiles do not play a role in the reduction processes and so they are not taken into account when determining the stoichiometric amounts of reductant needed in the process. Nevertheless, upon moving to the gas phase the volatile matter increases the surface area for

sufficient slag and reductant reaction [86]. Moreover, compared to the coke and biochar pyrolyzed at 1200 °C, more CO_2 is produced by the biochar pyrolyzed at 600 °C, which quickly reacts with solid carbon as shown in Equation (14) (Boudouard reaction). The generated CO also takes part in the reduction. Since reduction with solid carbon is slower than with CO, the higher amount of CO present during biochar reduction increases its effectiveness as reductant compared to coke [103].

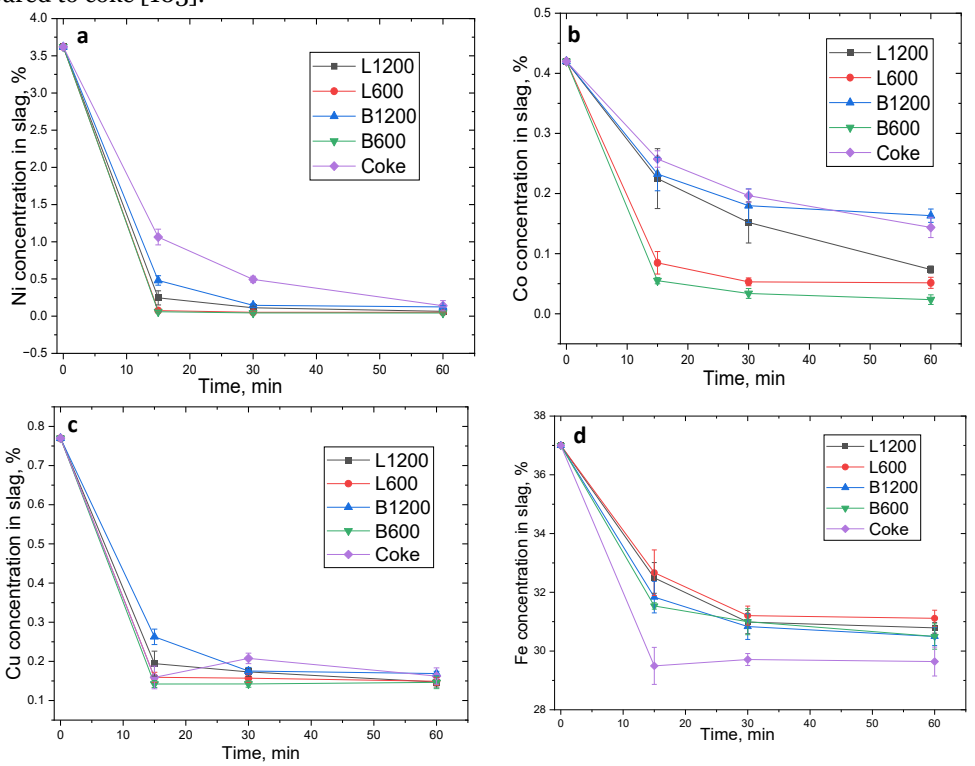

Figure 16. Concentrations of (a) nickel, (b) cobalt, (c) copper, and (d) iron in slag as a function of time during nickel slag reduction with L1200, L600, B1200, B600 biochars, and metallurgical coke. This figure is reproduced from Publication III, © 2023 Journal of Sustainable Metallurgy.

4.3.1 Distribution coefficient of elements during nickel slag reduction

The distribution coefficient gives an indication of the progress of the reduction reaction. The behavior of metal elements between the metal alloy and slag phase is estimated using the metal to slag distribution coefficient. A higher distribution coefficient implies that more of the element deports to the alloy.

The distribution coefficient, L, of an element, Me, between metal and slag phases was calculated using Equation (17):

$$L^{metal/slag} = \frac{wt\%\ Me\ in\ metal}{wt\%\ Me\ in\ slag} \quad (17)$$

The distribution coefficient of some elements: nickel, cobalt, copper, and iron, between metal alloy and slag as time progressed is depicted in Figure 17. The results obtained from this study have been compared to those estimated by Dańczak *et al.* [104], who used graphite from battery scrap as reductant. Comparisons are also made to the work of Avarmaa *et al.* [59] where a mixture of battery scrap and biochar was used as reductant for nickel slag reduction.

Overall, the distribution coefficients of all the metals when different reductants were employed increased with time. Since the distribution coefficient values rose only slightly, it can be inferred that the reduction progresses swiftly, and the metal oxides are effectively reduced to alloy after only 15 minutes of reduction. The highest distribution coefficients for nickel, cobalt, and iron were achieved when B600 biochar was employed as reductant, while the use of coke resulted in the lowest. This is because coke exhibits slower reaction kinetics compared to the different biochars.

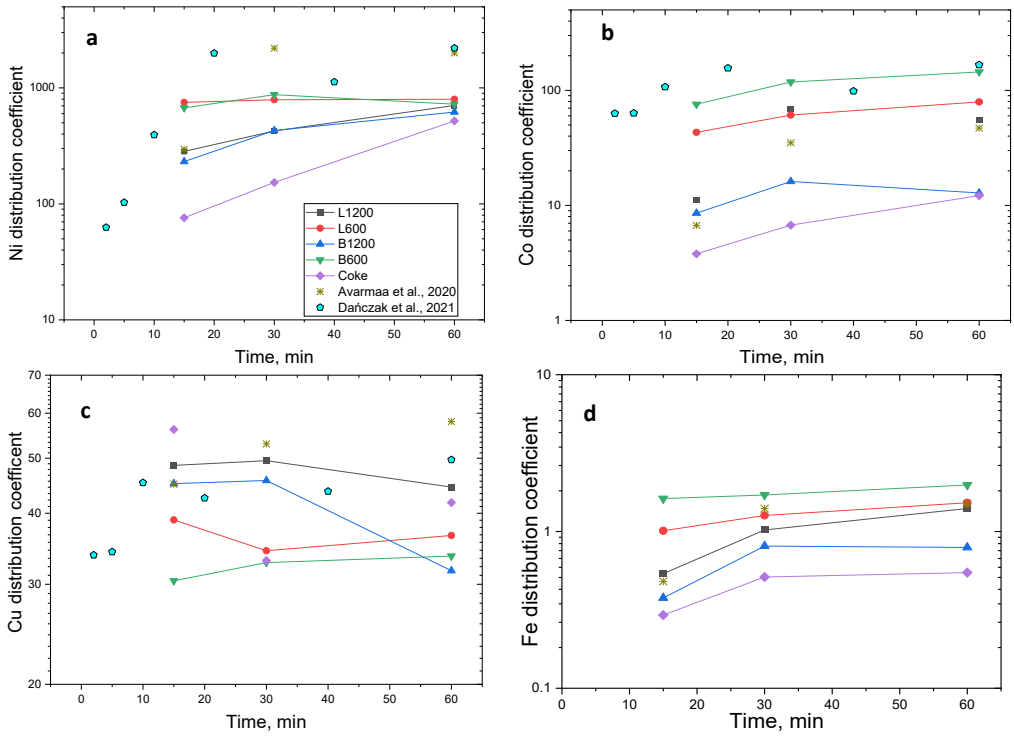

Figure 17. Metal alloy to slag distribution coefficient of (a) Ni, (b) Co, (c) Cu, and (d) Fe as a function of time at 1400 ℃. This figure is reproduced from Publication III, © 2023 Journal of Sustainable Metallurgy.

4.3.2 Thermodynamic simulation of nickel slag reduction with biochar

The effect on nickel slag reduction of using different masses of biochar as well as that of temperature was studied with FactSage™. The calculations were made using the composition of nickel slag from XRF analysis, and the ultimate and ash analyses of biochar.

Figure 18 shows the phases predicted by FactSage when one gram of nickel slag is reduced by different amounts of biochar. It can be seen that, when higher amounts of biochar are employed as reductant up to about 0.1 g, the mass of the slag continues to decrease and the mass of metal and gas increases.

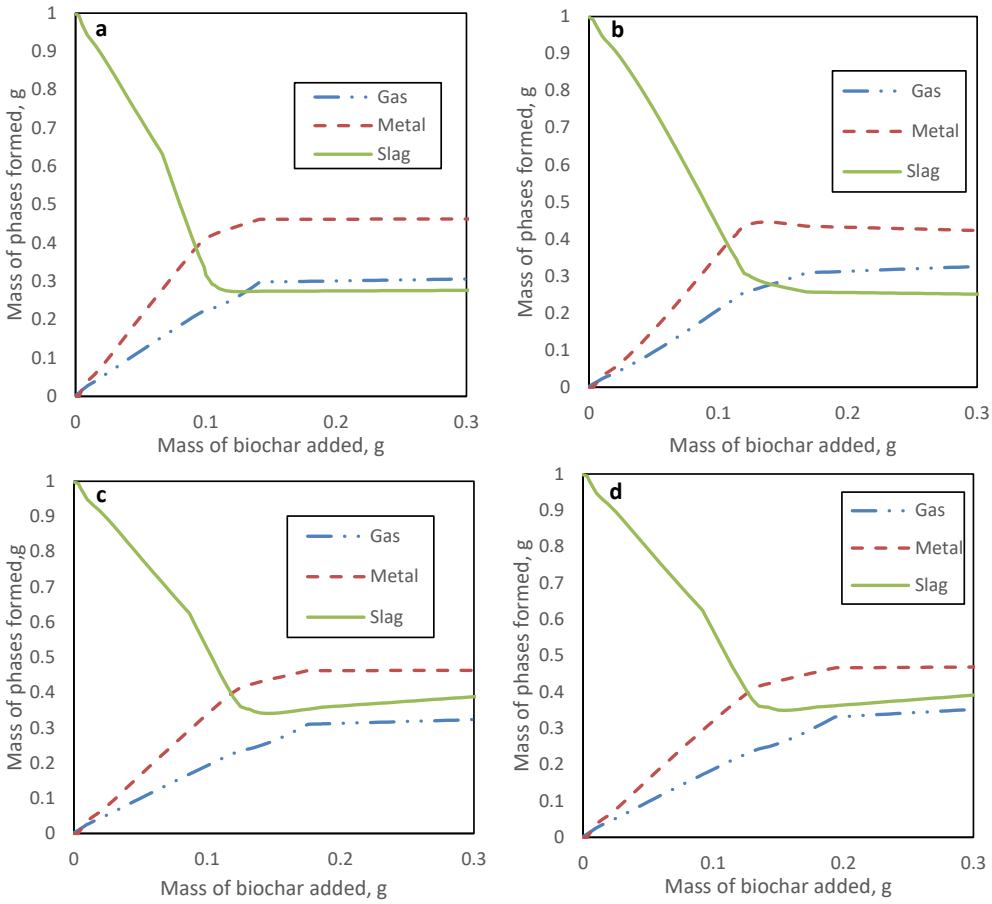

Figure 18. Formation of gas, metal, and slag phases during nickel slag reduction with varying additions of (a) L1200 (b) L600, (c) B1200, and (d) B600 biochars to 1 g of nickel slag at 1400 ℃ as predicted by FactSage™. This figure is reproduced from Publication III, © 2023 Journal of Sustainable Metallurgy.

The effect of temperature on nickel slag reduction was studied from 800 ℃ to 1600 ℃. The masses of the different phases that are produced during nickel slag reduction with B600 biochar at different temperatures is shown in Figure 19. It can be observed that the sample begins to melt and form liquid slag at temperatures above 1150 ℃. At temperatures greater than 1390 ℃, the sample is completely molten because other solid phases like spinel and olivine are absent. FactSage™ predicts the formation of gas and liquid metal phases as well in this temperature range.

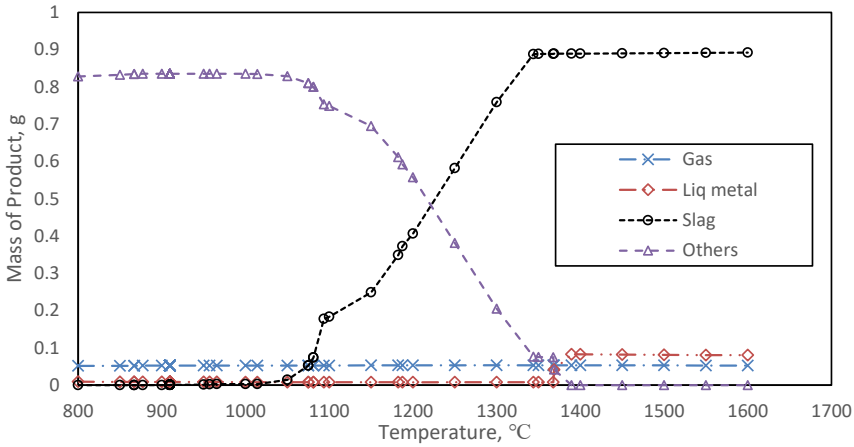

Figure 19. Formation of gas, liquid metal, slag, and other phases (FCC, spinel, and olivine) during nickel slag reduction with B600 biochar at different temperatures as predicted by FactSage™. This figure is reproduced from Publication III, © 2023 Journal of Sustainable Metallurgy.

4.3.3 Mass balance calculations of nickel slag reduction

Mass balance calculations have been done to account for the masses of each of the elements during reduction experiment. This calculation was based on the results obtained from Factsage modeling. It was assumed that the reduction reaction during had progressed to equilibrium and the amount of the metal element that volatilize to the gas phase is negligible. The ratio of slag to metal obtained from Factsage calculations were used.

The mass percent of an element, Me, in the reduced nickel slag sample is calculated as:

$$M_{Me(Total)} = M_{Me(EPMA,metal)} \times m_{Me(Factsage,metal)} + M_{Me(EPMA,slag)} \times m_{Me(Factsage,slag)} \quad (18)$$

Where $M_{Me(Total)}$ is the mass percent of Me in the sample, $M_{Me(EPMA,metal)}$ is the mass percent of Me in metal alloy phase from EPMA analysis, $m_{Me(Factsage,metal)}$ is the mass fraction of metal in Factsage calculations, $M_{Me(EPMA,slag)}$ is the mass percent of Me in the slag phase from EPMA analysis and $m_{Me(Factsage,slag)}$ is the mass fraction of slag in Factsage calculations.

The percentage of Me that deports to the metal phase is calculated as:

$$M_{Me(metal)} = \frac{M_{Me(EPMA,metal)} \times m_{Me(Factsage,metal)}}{M_{Me(Total)}} \times 100\% \quad (19)$$

The percentage of Me that remains in the slag phase is calculated as:

$$M_{Me(metal)} = \frac{M_{Me(EPMA,slag)} \times m_{Me(Factsage,slag)}}{M_{Me(Total)}} \times 100\% \quad (20)$$

The mass balance for the main metal elements; Fe, Ni, Co and Cu for nickel slag reduction for biochar and coke reduction are presented in Figure 20. Mass balance calculations show that when biochar B600 is used as reductant, more than 10% of Fe in the original slag is reduced to the metal phase after 15 min of reduction. On the other hand, after 60 minutes, about 4% of Fe is present in the metal phase during nickel slag reduction with coke.

Figure 20. Percentage of iron, nickel, copper and cobalt in slag phase and metal alloy phase during nickel slag reduction with (a) B600 for 15 min, (b) B600 for 30 min, (c) B600 for 60 min, (d) B1200 for 15 min, (e) B1200 for 30 min, (f) B1200 for 60 min, (g) L600 for 15 min, (h) L600 for 30 min, (i) L600 for 60 min, (j) L1200 for 15 min, (k) L1200 for 30 min, (l) L1200 for 60 min, (m) Coke for 15 min, (n) Coke for 30 min, and (o) Coke for 60 min at 1400℃.

Moreover, less than 2% of nickel is present in the slag after reduction with B600 biochar while after 15 min of reduction experiment with coke about 15% if nickel is present in slag. The present of cobalt and copper and copper that deport to the metal alloy phase were higher in reduction experiments with biochar compared to that of coke. This confirms that biochar is a more effective reducing agent compared to coke.

4.4 Copper slag reduction with biochar

Biochar was also employed as reductant in copper slag treatment. The effect of time was investigated at 1250 °C for 15, 30, and 60 min and that of temperature was studied between 1250 °C and 1350 °C for a duration of 60 min. Figure 21 shows the SEM image of the polished cross-sections of the sample obtained from reduction with L600 biochar.

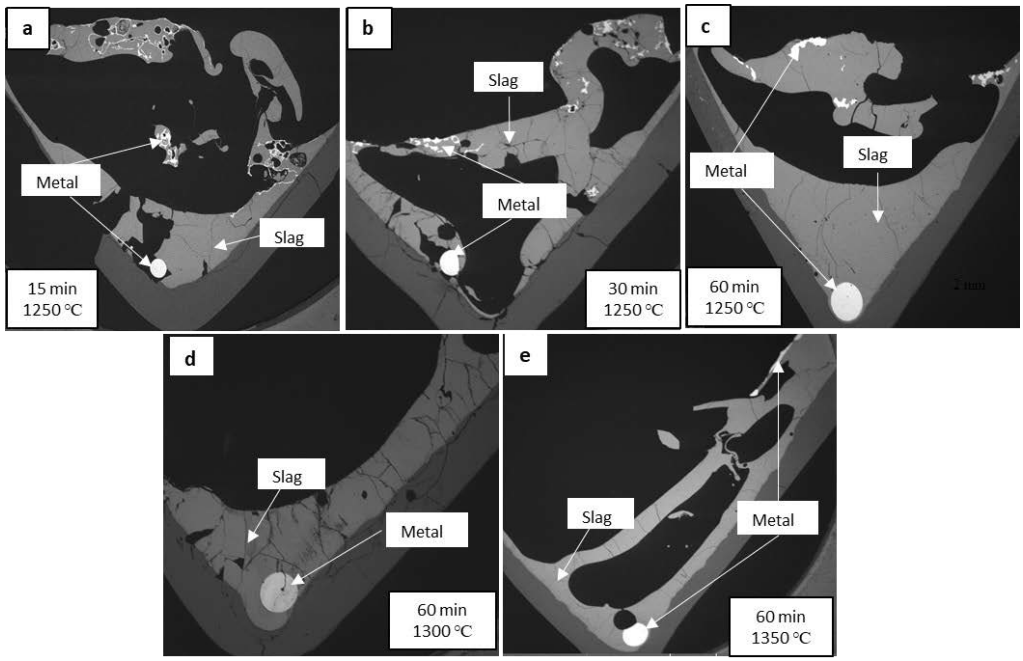

Figure 21. SEM micrographs of polished cross-sections of copper slag reduction samples with L600 at (a)1250 °C for 15 minutes, (b) 1250 °C for 30 minutes, (c) 1250 °C for 60 minutes, (d) 1300 °C for 60 minutes, and (e) 1350 °C for 60 minutes. This figure is reproduced from Publication IV, © 2024 Journal of Sustainable Metallurgy.

It can be seen that metal alloy droplets (bright regions) are produced during the reduction experiment. Metal alloy droplets are typically found both at the top and bottom of the slag. After analyzing the sample, it was found that the metal droplets at the top were almost entirely composed of pure iron (>90 wt%), whereas the metal droplets at the bottom contained iron and significantly higher amounts of other metals, particularly copper and arsenic. Moreover, FactSage™ predicts that both solid and liquid metal are stable at the experimental temperature. The solid metal phase, predominantly iron, stays at the top edge of the slag. The solid metal alloy has a high liquidus temperature and thus may form mushy rafts that have difficulty settling through the slag layer.

Figure 22 and Figure 23 show the concentrations of some elements in the slag as a function of reaction duration and temperature, respectively. The concentrations of copper, nickel, and arsenic in the slag decreased significantly (~90%) within 15 minutes of reduction. It is expected that increasing the time should result in the increased reduction of slag. However, it can be inferred that, although a longer reaction duration increases the reduction of iron oxide from the slag, the removal of other metal elements, such as copper and arsenic, is not improved.

While the concentration of metals in the slag was significantly lower than the original copper slag sample (see Figure 23), increasing the temperature from 1250 °C to 1350 °C did not significantly improve the removal of metals from the slag.

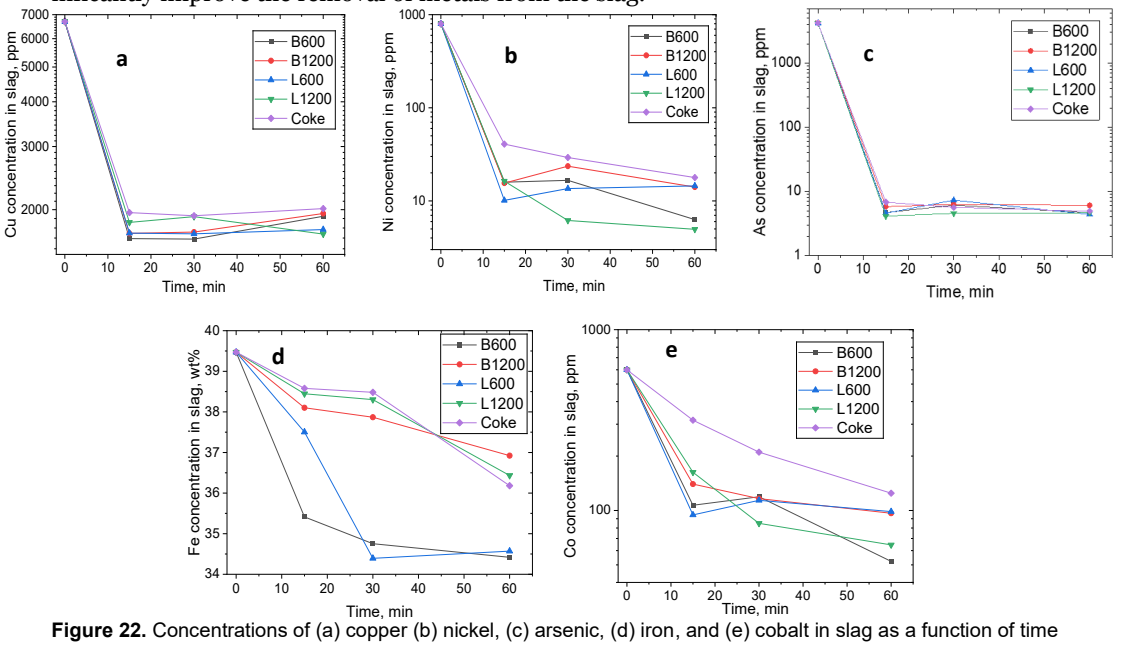

Figure 22. Concentrations of (a) copper (b) nickel, (c) arsenic, (d) iron, and (e) cobalt in slag as a function of time during copper slag reduction with B600, B1200, L600, L1200 biochars, and metallurgical coke. This figure is reproduced from Publication IV, © 2024 Journal of Sustainable Metallurgy.

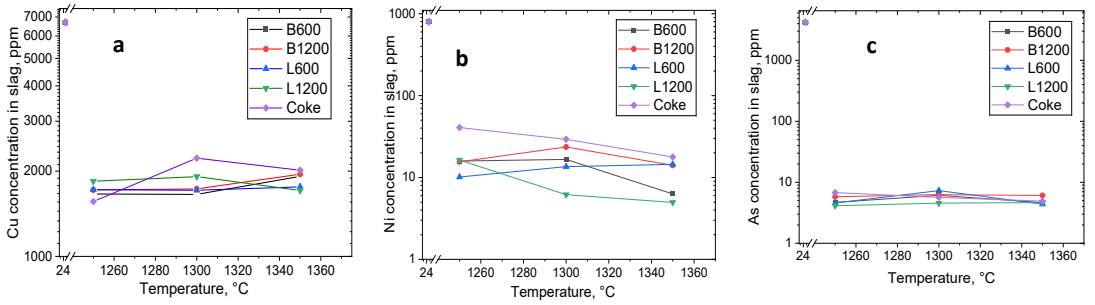

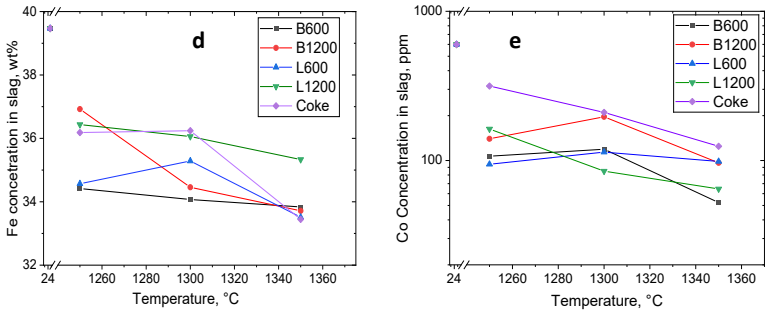

Figure 23. Concentrations of (a) copper, (b) nickel, (c) arsenic, (d) iron, and (e) cobalt in slag as a function of temperature during copper slag reduction with B600, B1200, L600, L1200 biochars, and metallurgical coke for 60 minutes. This figure is reproduced from Publication IV, © 2024 Journal of Sustainable Metallurgy.

4.4.1 Distribution coefficient of elements during copper slag reduction

The metal to slag distribution coefficient of selected metal elements (Cu, Ni, As, Fe, and Co) during the reduction of copper smelting slag at 1250 °C was calculated using Equation (17) and the logarithm is shown in Figure 24. The results from the calculations were compared with the results from Rinne *et al.* [105]. In their work, the metals that were recovered from the flotation fraction of industrial lithium-ion battery scrap were utilized in copper slag reduction at 1300 °C. It can be observed that the results from using biochar as reductant are similar to those of Rinne *et al.*

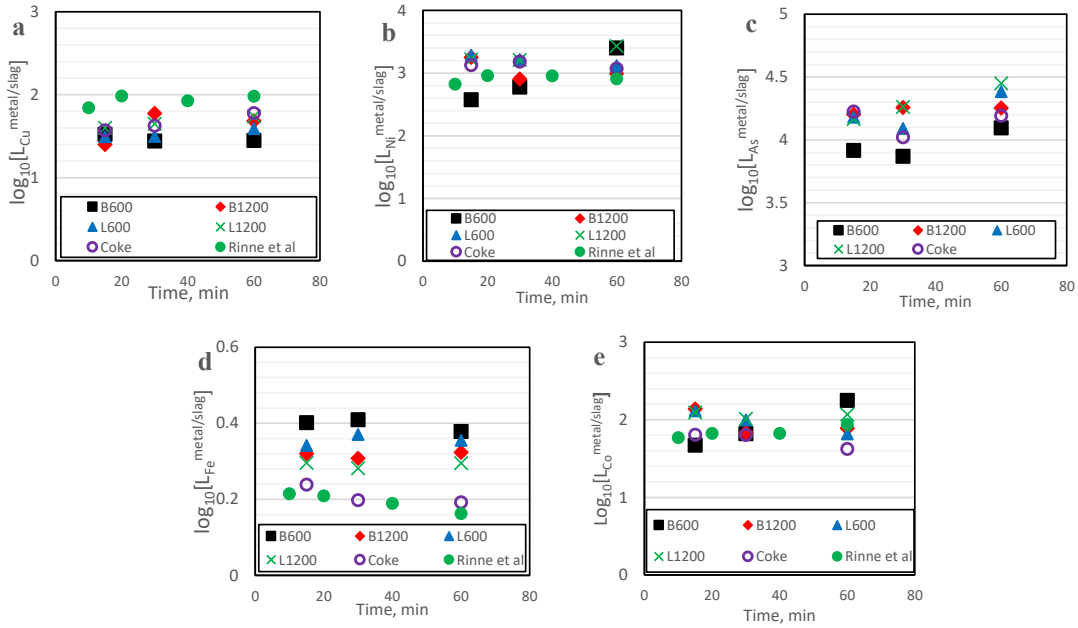

Figure 24. Distribution coefficients of (a) copper (b) nickel, (c) arsenic, (d) iron, and (e) cobalt between metal and slag as a function of time during copper slag reduction with B600, B1200, L600, L1200 biochars, and coke at 1250 °C. This figure is reproduced from Publication IV, © 2024 Journal of Sustainable Metallurgy.

4.4.2 Thermodynamic simulation of copper slag reduction with biochar

HSC Chemistry and FactSage™ were employed to perform thermodynamic calculations to simulate copper slag reduction. The standard Gibbs energy change was calculated to determine the reactions that are feasible at the experimental temperature as well as the sequence of reactions. Figure 25 shows the standard Gibbs energy from 700 °C to 1500 °C. HSC provides information the behavior of elements assuming they are in standard state. Although the slag reduction is complex, results from HSC calculations may help to understand the behavior of each element in the complex system and can be used as a reference to compare the properties of the different elements.

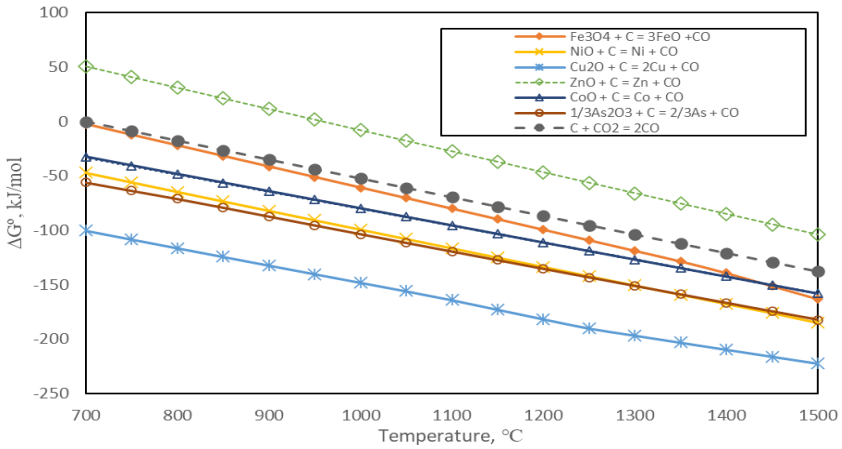

Figure 25. Standard Gibbs energy of reactions that may take place during copper slag reduction from 700 °C to 1500 °C. This figure is reproduced from Publication IV, © 2024 Journal of Sustainable Metallurgy.

FactSage™ was used to study the effect of reducing one gram of copper slag with different amounts of biochar. As shown in Figure 26, increasing the amount of biochar increases the metal content and the amount of gas. This indicates that the reduction degree rises with the addition of more biochar.

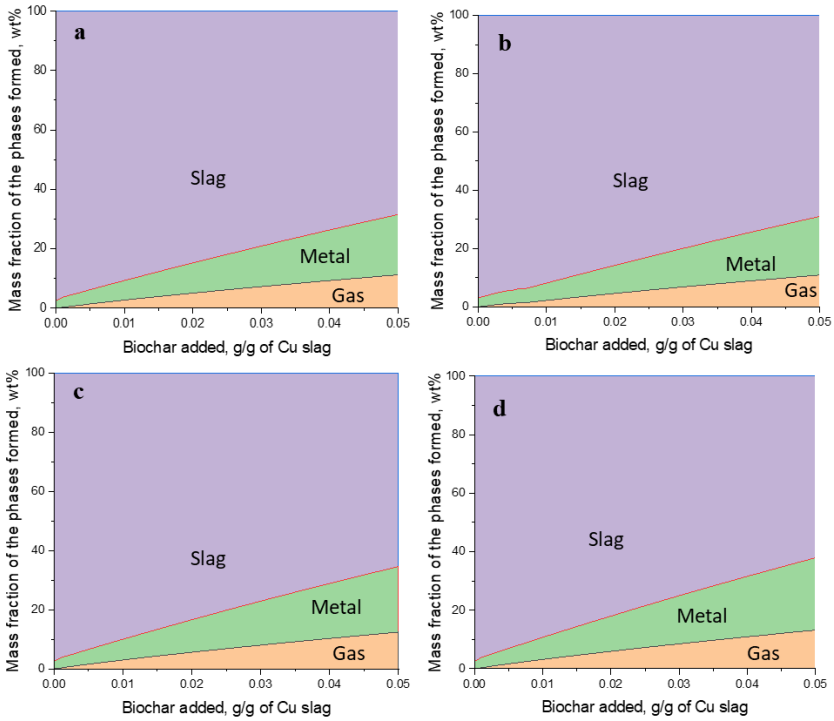

Figure 26. Different phases formed during copper slag reduction with varying addition up to 0.05 g of (a) B600, (b) B1200, (c) L600, and (d) L1200 biochar per gram of copper smelting slag at 1250 °C as predicted by FactSage™.

Figure 27 shows the products generated at different temperatures during copper smelting slag reduction. The calculations predict the presence of fayalite and spinel at lower temperatures up to about 1150 °C. This confirms the XRD analysis which shows that the slag contains fayalite and spinel. Solid metal is produced during reduction at lower temperatures and is absent only after 1350 °C, although liquid metal is formed at temperatures greater than 900 °C. This validates the experimental findings where two metal phases were generated. Moreover, FactSage™ predicts that the solid metal phase primarily is composed of iron, which confirms the experimental results.

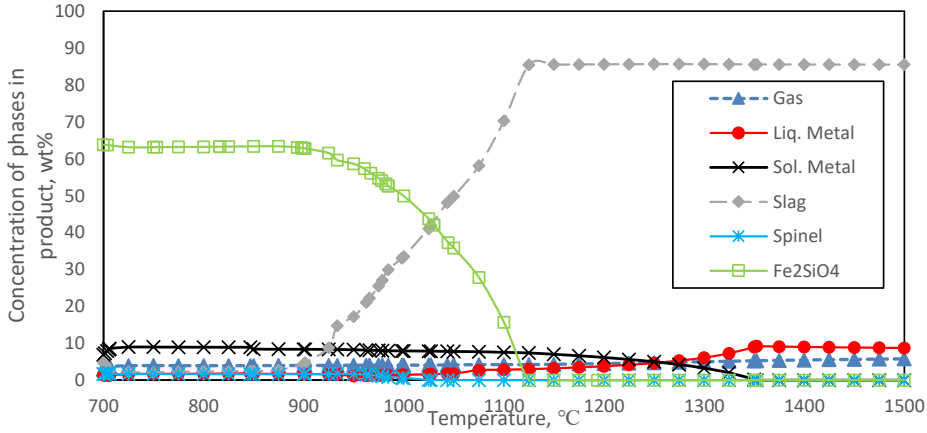

Figure 27. Formation of gas, liquid metal, solid metal slag, spinel, and Fe_2SiO_4 phases during copper slag reduction of 1 g industrial copper slag with 0.02 g B600 biochar at different temperatures, as predicted by FactSage™. This figure is reproduced from Publication IV, © 2024 Journal of Sustainable Metallurgy.

4.4.3 Mass balance calculations of copper slag reduction

Mass balance for copper reduction experiments were calculated using the same method as nickel slag reduction. It was based on the metal to slag ratio obtained from Factsage calculations. Figure 28 shows the mass balance for the metal elements Fe, Ni, Co and Cu.

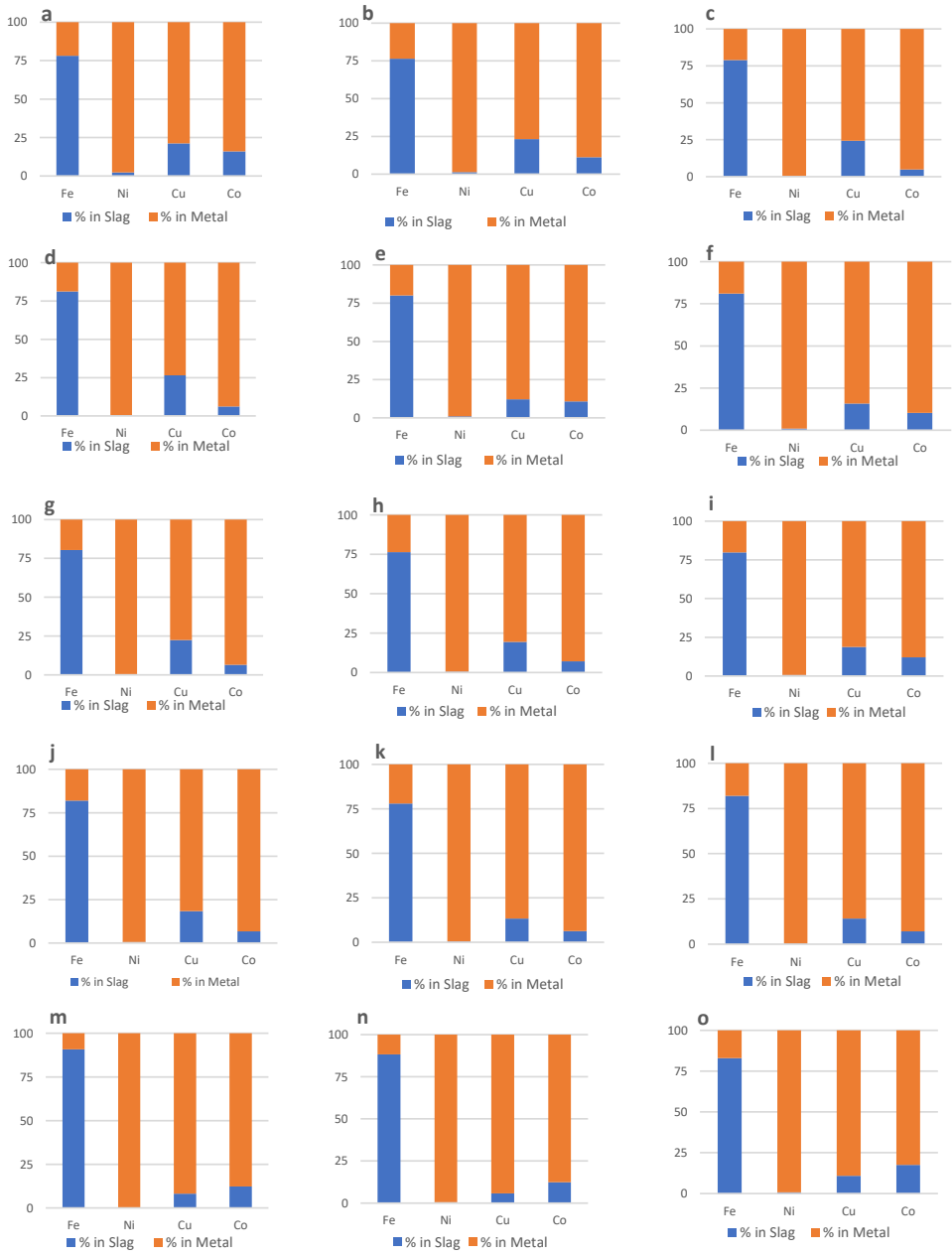

Figure 28. Percentage of iron, nickel, copper and cobalt in slag phase and metal alloy phase during copper slag reduction with (a) B600 for 15 min, (b) B600 for 30 min, (c) B600 for 60 min, (d) B1200 for 15 min, (e) B1200 for 30 min, (f) B1200 for 60 min, (g) L600 for 15 min, (h) L600 for 30 min, (i) L600 for 60 min, (j) L1200 for 15 min, (k) L1200 for 30 min, (l) L1200 for 60 min, (m) Coke for 15 min, (n) Coke for 30 min, and (o) Coke for 60 min at 1400℃.

After 15 min of copper slag reduction experiments for all the reducing agents, it is observed that almost all the nickel is present in the metal phase. This can be attributed to the low concentration in the original slag. Less than 10% of Fe is present in the metal alloy for reduction with coke while B600 biochar reduced about 20% to the metal alloy phase.

5. Conclusions

As the metallurgical industry targets greener and more efficient practices, the use of alternative reductants in high temperature processes has the potential to achieve both economic and environmental sustainability goals. In this thesis work, several alternative reductants were applied in high temperature processes for metal recovery from secondary sources. Printed circuit board leach residue was employed as reductant for the solid-state reduction of hematite in DSC-TGA coupled with QMS. Zinc leach residue was reduced with hydrogen while biochar was utilized for nickel and copper smelting slag reduction on laboratory scale in a vertical furnace. The feasibility of adopting alternative reductants in ironmaking and pyrometallurgical treatment of secondary resources were determined in this study. The effect of the amount of reducing agent, reduction time, and temperature on the extent of reduction was investigated.

Analysis of the solid reductants i.e., biochar and PCB leach residue, showed that they had a higher volatile content compared with coke or graphite. While carbon is mainly responsible for the reduction of metal oxides, the relatively high volatile content also contributes to the reduction process. PCBs were shown to contain a high amount of ash attributed to the presence of glass fiber and ceramics in PCBs.

Hematite reduction was performed from room temperature to 1200 °C with PCBs, graphite, and their blends. PCBs were found to have faster reduction kinetics compared with graphite during hematite reduction. At temperatures below 1000 °C, the reduction efficiency increased when PCBs and PCB-graphite blends were used as reductants relative to reduction with graphite. This can be ascribed to the presence of hydrocarbons that take part in the reduction of hematite. FactSage™ simulations were carried out from 25 °C to 1500 °C for comparison with the products from the experiments. The simulations were in agreement with the results from the experiments and predicted that fayalite would be generated between 200 °C and 800 °C due to the high SiO_2 content.

Prior to the reduction of iron residue from zinc processing with hydrogen, the sample underwent pretreatment in air at 700 °C and oxidation. This was performed to lower the sulfur content to <1 wt%. After oxidation, the melt was reduced with hydrogen in a 20 vol% mixture with nitrogen at temperatures 1200 °C, 1250 °C, and 1300 °C. The results showed that hydrogen reduced the metal oxide to produce speiss droplets after 10 min. The small speiss droplets that were generated within the slag combined and sank to the bottom of the crucible. Two scenarios were considered during the thermodynamic modeling of the reduction of iron residue. FactSage™ was used to predict the products formed when the oxygen partial pressure was varied. The results showed the formation of two liquid metals and solid iron at $P(O_2) < 10^{-11}$, which corresponds to the result obtained from the experiment after the samples were left in the furnace for one hour under inert conditions after the reduction. In the second instance, the

product formed when hydrogen was reacted with the sample was predicted by FactSage™. Several repeated calculations were made where the gas produced was excluded from the system and hydrogen was reacted with the rest of the sample. This was done to simulate the reduction reaction taking place in the furnace where hydrogen is continuously supplied to the furnace and reacted gas exits through exhaust gas.

During reduction of nickel slag at 1400 °C, four different biochars, black pellets and lignin, each pyrolyzed at 600 °C and 1200 °C were used as reductants. Although the biochars pyrolyzed at 1200 °C contained higher amounts of carbon, the biochar pyrolyzed at 600 °C appeared to be more reactive. B600, i.e., the black pellets pyrolyzed at 600 °C, was the most effective biochar. Nickel slag was treated with coke for comparison, and it was revealed that biochar had faster reaction kinetics than coke. This may be due to the higher volatile matter and the dominant Boudouard reaction. Mass balance calculations were performed based on the results from Factsage and EPMA analysis. It was revealed that almost all nickel deports to the metal phase apart from reduction with coke. In addition, more than 10% of the iron in the original slag is reduced to the metal alloy phase during reduction with B600 biochar. Mass balance calculation also confirm that biochar is more effective compared to coke.

The effect of time and temperature was studied for the different reductants in high temperature copper slag cleaning. The results indicated that most of the reduction took place within the first few minutes because there was sufficient contact between the slag and reductant. The reduction rate progressed as the duration was increased but at a lower rate. Moreover, as the temperature was increased, the metal atoms easily migrated resulting in the growth of metallic alloy which settled at the bottom of the crucible. The results indicated that biochar was more effective than coke, particularly at lower temperature. The thermodynamic calculations of nickel slag reduction and copper slag reduction using FactSage™ were in agreement with the experiments. In copper slag reduction, HSC Chemistry was used to calculate the standard Gibbs energy of the reactions taking place and the sequence of the reduction reactions. It was shown that the reactions were feasible at the experimental temperatures. Mass balance of some metal elements was also calculated for copper slag reduction experiment. Between 10% and 20% of the iron in the original slag migrates to the metal alloy phase. The calculations also show that Nickel is present mainly in the metal alloy phase due to its low concentration in the initial slag.

In recent years, extensive studies have been performed on the use of non-fossil reductants in pyrometallurgical operations. This work utilized alternative reductants with the dual aim of decreasing CO_2 emissions in the environment and recovering metals from waste sources. The data obtained from the experiments in this thesis is beneficial for science and industry. The application of biochar is advantageous from an industrial perspective due to the shorter reduction time and lower carbon emissions compared with coke. Some challenges, such as low volume density, high moisture content, expensive transportation and storage, and poor grindability, are associated with biobased reductants, which can be mitigated by using briquetting and pyrolysis. Since biochar is more reactive than coke, further studies can be performed on the use of biochar in slag treatment at lower temperatures. It has been mentioned that, since the cost of production of biochar reductants is high, carbon taxes need to be imposed to incentivize the use of non-fossil reductants [59]. Economic studies could be done in order to smoothen the transition from conventional reductants to non-fossil reductants.

References

1. Zhang, P., & Guo, Q. (2023). Carbon Emission Reduction Effects of China's Green Local Government Special Bonds under 'Dual Carbon Goals.' *Finance Research Letters*, *58*. https://doi.org/10.1016/j.frl.2023.104348
2. Yilmaz, C., Wendelstorf, J., & Turek, T. (2017). Modeling and simulation of hydrogen injection into a blast furnace to reduce carbon dioxide emissions. *Journal of Cleaner Production*, *154*, 488–501. https://doi.org/10.1016/j.jclepro.2017.03.162
3. European commission. (2019). *A STRATEGIC LONG-TERM VISION FOR A PROSPEROUS, MODERN, COMPETITIVE AND CLIMATE-NEUTRAL EU ECONOMY Climate Action*. https://data.europa.eu/doi/10.2834/02074
4. Orth, A., Anastasijevic, N., & Eichberger, H. (2007). Low CO2 emission technologies for iron and steelmaking as well as titania slag production. *Minerals Engineering*, *20*. https://doi.org/10.1016/j.mineng.2007.02.007
5. Bailera, M., Lisbona, P., Peña, B., & Romeo, L. M. (2021). A review on CO2mitigation in the Iron and Steel industry through Power to X processes. In *Journal of CO2 Utilization* 46. https://doi.org/10.1016/j.jcou.2021.101456
6. Yang, J., Li, L., Liang, Z., Peng, X., Deng, X., Li, J., Yi, L., Huang, B., & Chen, J. (2023). Direct reduction of iron ore pellets by H2-CO mixture: An in-situ investigation of the evolution and dynamics of swelling. *Materials Today Communications*, *36*. https://doi.org/10.1016/j.mtcomm.2023.106940
7. Shahabuddin, M., Brooks, G., & Rhamdhani, M. A. (2023). Decarbonisation and hydrogen integration of steel industries: Recent development, challenges and technoeconomic analysis. In *Journal of Cleaner Production* 395. https://doi.org/10.1016/j.jclepro.2023.136391
8. Deng, J., Ning, X., Shen, J., Ou, W., Chen, J., Qiu, G., Wang, Y., & He, Y. (2022). Biomass waste as a clean reductant for iron recovery of iron tailings by magnetization roasting. *Journal of Environmental Management*, *317*. https://doi.org/10.1016/j.jenvman.2022.115435
9. Guilbert, D., & Vitale, G. (2021). Hydrogen as a Clean and Sustainable Energy Vector for Global Transition from Fossil-Based to Zero-Carbon. In *Clean Technologies* 3(4), 881–909. https://doi.org/10.3390/cleantechnol3040051
10. Liu, W., Zuo, H., Wang, J., Xue, Q., Ren, B., & Yang, F. (2021). The production and application of hydrogen in steel industry. In *International Journal of Hydrogen Energy* 46(17), l0548–10569. https://doi.org/10.1016/j.ijhydene.2020.12.123
11. Sommerfeld, M., & Friedrich, B. (2021). Replacing fossil carbon in the production of ferroalloys with a focus on bio-based carbon: A review 11(11). https://doi.org/10.3390/min11111286
12. Jandieri, G. (2023). Increasing the efficiency of secondary resources in the mining and metallurgical industry. *The Journal of the Southern African Institute of Mining and Metallurgy*, *123*(1), 1–8. https://doi.org/10.17159/2411-9717/1092/2023
13. Ghisellini, P., Cialani, C., & Ulgiati, S. (2016). A review on circular economy: The expected transition to a balanced interplay of environmental and economic systems. *Journal of Cleaner Production*, *114*, 11–32. https://doi.org/10.1016/j.jclepro.2015.09.007
14. Zhou, S., Wei, Y., Li, B., & Wang, H. (2019). Cleaner recycling of iron from waste copper slag by using walnut shell char as green reductant. *Journal of Cleaner Production*, *217*, 423–431. https://doi.org/10.1016/j.jclepro.2019.01.184

15. Holland, K., Eriç, R. H., Taskinen, P., & Jokilaakso, A. (2019). Upgrading copper slag cleaning tailings for re-use. *Minerals Engineering*, *133*, 35–42. https://doi.org/10.1016/j.mineng.2018.12.026
16. Sun, W., Li, X., Liu, R., Zhai, Q., & Li, J. (2021). Recovery of valuable metals from nickel smelting slag based on reduction and sulfurization modification. *Minerals*, *11*(9), 1–14. https://doi.org/10.3390/min11091022
17. Zhang, G., Wang, N., Chen, M., & Cheng, Y. (2020). Recycling nickel slag by aluminum dross: Iron-extraction and secondary slag stabilization. *ISIJ International*, *60*(3), 602–609. https://doi.org/10.2355/isijinternational.ISIJINT-2019-173
18. Mombelli, D., Mapelli, C., Barella, S., Gruttadauria, A., & Spada, E. (2019). Jarosite wastes reduction through blast furnace sludges for cast iron production. *Journal of Environmental Chemical Engineering*, *7*(2). https://doi.org/10.1016/j.jece.2019.102966
19. Zhou, W., Liu, X., Lyu, X., Gao, W., Su, H., & Li, C. (2022). Extraction and separation of copper and iron from copper smelting slag: A review. In *Journal of Cleaner Production* 368. Elsevier Ltd. https://doi.org/10.1016/j.jclepro.2022.133095
20. Alp, I., Deveci, H., & Süngün, H. (2008). Utilization of flotation wastes of copper slag as raw material in cement production. *Journal of Hazardous Materials*, *159*(3), 390–395. https://doi.org/10.1016/j.jhazmat.2008.02.056
21. Gorai, B., Jana, R. K., & Premchand. (2003). Characteristics and utilisation of copper slag - A review. *Resources, Conservation and Recycling*, *39*(4), 299–313. https://doi.org/10.1016/S0921-3449(02)00171-4
22. Rämä, M., Klemettinen, L., Rinne, M., Taskinen, P., Michallik, R. M., Salminen, J., & Jokilaakso, A. (2023). Processing of a Zinc Leach Residue by a Non-Fossil Reductant. *ACS Omega*, *8*(24), 21450–21463. https://doi.org/10.1021/acsomega.3c00250
23. Roy, S., Datta, A., & Rehani, S. (2015). Flotation of copper sulphide from copper smelter slag using multiple collectors and their mixtures. *International Journal of Mineral Processing*, *143*, 43–49. https://doi.org/10.1016/j.minpro.2015.08.008
24. Sibanda, V., Sipunga, E., Danha, G., & Mamvura, T. A. (2020). Enhancing the flotation recovery of copper minerals in smelter slags from Namibia prior to disposal. *6*(1). https://doi.org/10.1016/j.heliyon.2019.e03135
25. Guo, Z., Zhu, D., Pan, J., Wu, T., & Zhang, F. (2016). Improving Beneficiation of Copper and Iron from Copper Slag by Modifying the Molten Copper Slag. *Metals*, *6*(4), 86-98. https://doi.org/10.3390/met6040086
26. Herreros, O., Quiroz, R., Manzano, E., Bou, C., & Viñals, J. (1998). Copper extraction from reverberatory and flash furnace slags by chlorine leaching. *Hydrometallurgy*, *49*(2), 87–101. https://doi.org/10.1016/s0304-386x(98)00010-3
27. Nadirov, R. K. (2019). Recovery of Valuable Metals from Copper Smelter Slag by Sulfation Roasting. *Transactions of the Indian Institute of Metals*, *72*(3), 603–607. https://doi.org/10.1007/s12666-018-1507-5
28. Patrick, J., Prasetyo, A. B., Munir, B., Maksum, A., & Soedarsono, J. W. (2018). The effect of addition of sodium sulphate (Na2SO4) to nickel slag pyrometallurgical process with temperature and additives ratio as variables. *67*, 1–8. https://doi.org/10.1051/e3sconf/20186703053
29. Heo, J. H., Chung, Y., & Park, J. H. (2016). Recovery of iron and removal of hazardous elements from waste copper slag via a novel aluminothermic smelting reduction (ASR) process. *Journal of Cleaner Production*, *137*, 777–787. https://doi.org/10.1016/j.jclepro.2016.07.154
30. Yao, G., Guo, Q., Li, Y., Xu, Z., Han, Z., He, M., & Qi, T. (2022). An innovation technology for recovering silver and valuable metals from hazardous zinc leaching residue through direct reduction. *Minerals Engineering*, *188*. https://doi.org/10.1016/j.mineng.2022.107857
31. Shen, H., & Forssberg, E. (2003). An overview of recovery of metals from slags. *Waste Management*, *23*(10), 933–949. https://doi.org/10.1016/S0956-053X(02)00164-2

32. Li, Q., Yang, F., Wang, Z., & Liu, S. (2019). Study on Mechanism of Oxidation Modification of Copper Slag. *Transactions of the Indian Institute of Metals*, *72*(12), 3223–3231. https://doi.org/10.1007/s12666-019-01788-9
33. Creedy, S., Glinin, A., Matusewicz, R., Hughes, S., & Reuter, M. (2013). Outotec ® Ausmelt Technology for Treating Zinc Residues. *World of Metallurgy - ERZMETALL*, *66*(4), 230–235.
34. Dawood, F., Anda, M., & Shafiullah, G. M. (2020). Hydrogen production for energy: An overview. In *International Journal of Hydrogen Energy.* 45(7) 3847–3869. https://doi.org/10.1016/j.ijhydene.2019.12.059
35. Parra, D., Valverde, L., Pino, F. J., & Patel, M. K. (2019). A review on the role, cost and value of hydrogen energy systems for deep decarbonisation. In *Renewable and Sustainable Energy Reviews* 101, 279–294. https://doi.org/10.1016/j.rser.2018.11.010
36. Acar, C., & Dincer, I. (2014). Comparative assessment of hydrogen production methods from renewable and non-renewable sources. In *International Journal of Hydrogen Energy* 39(1) 1–12. https://doi.org/10.1016/j.ijhydene.2013.10.060
37. Heidari, A., Niknahad, N., Iljana, M., & Fabritius, T. (2021). A review on the kinetics of iron ore reduction by hydrogen. In *Materials* 14(24). https://doi.org/10.3390/ma14247540
38. Li, F., Chu, M., Tang, J., Liu, Z., Zhou, Y., & Wang, J. (2021). Exergy analysis of hydrogen-reduction based steel production with coal gasification-shaft furnace-electric furnace process. *International Journal of Hydrogen Energy*, *46*(24), 12771–12783. https://doi.org/10.1016/j.ijhydene.2021.01.083
39. Luidold, S., & Antrekowitsch, H. (2007). Hydrogen as a Reducing Agent : State-of-the-Art Science and Technology. *Journal of the Minerals, Metals & Materials Society*, *59*(6), 20–26. https://doi.org/10.1007/s11837-007-0072-x
40. Dong, H., Li, R., Zhao, W., Zhang, Y., Chen, X., Zhang, Q., Cao, M., & Liu, F. (2023). Chemical kinetics properties and the influences of different hydrogen blending ratios on reactions of natural gas. *Case Studies in Thermal Engineering*, *41*. https://doi.org/10.1016/j.csite.2022.102676
41. Spreitzer, D., & Schenk, J. (2019). Reduction of Iron Oxides with Hydrogen — A Review. *Steel Research International*, *1900108*, 1–17. https://doi.org/10.1002/srin.201900108
42. Ma, K., Deng, J., Wang, G., Zhou, Q., & Xu, J. (2021). Utilization and impacts of hydrogen in the ironmaking processes: A review from lab-scale basics to industrial practices. In *International Journal of Hydrogen Energy.* 46(52) 26646–26664. https://doi.org/10.1016/j.ijhydene.2021.05.095
43. Dang, J., Chou, K.-C., Hu, X.-J., & Zhang, G.-H. (2013). Reduction Kinetics of Metal Oxides by Hydrogen. *Steel Research International*, *84*(6), 526–533. https://doi.org/10.1002/srin.201200242
44. SSAB, "HYBRIT®. A new revolutionary steelmaking technology." Accessed: Apr. 15, 2024. [Online]. Available: https://www.ssab.com/en/fossil-free-steel/insights/hybrit-a-new-revolutionary-steelmaking-technology
45. Luo, M., Yi, Y., Wang, S., Wang, Z., Du, M., Pan, J., & Wang, Q. (2018). Review of hydrogen production using chemical-looping technology. In *Renewable and Sustainable Energy Reviews* 81, 3186–3214. Elsevier Ltd. https://doi.org/10.1016/j.rser.2017.07.007
46. Al-Zareer, M., Dincer, I., & Rosen, M. A. (2020). Production of hydrogen-rich syngas from novel processes for gasification of petroleum cokes and coals. *International Journal of Hydrogen Energy*, *45*(20), 11577–11592. https://doi.org/10.1016/j.ijhydene.2019.10.108
47. Kothari, R., Buddhi, D., & Sawhney, R. L. (2008). Comparison of environmental and economic aspects of various hydrogen production methods. In *Renewable and Sustainable Energy Reviews* 12(2), 553–56). https://doi.org/10.1016/j.rser.2006.07.012
48. Kaya, M. F., Demir, N., Albawabiji, M. S., & Taş, M. (2017). Investigation of alkaline water electrolysis performance for different cost effective electrodes under magnetic field. *International Journal of Hydrogen Energy*, *42*(28), 17583–17592. https://doi.org/10.1016/j.ijhydene.2017.02.039

49. Kovač, A., Marciuš, D., & Budin, L. (2019). Solar hydrogen production via alkaline water electrolysis. *International Journal of Hydrogen Energy*, *44*(20), 9841–9848. https://doi.org/10.1016/j.ijhydene.2018.11.007
50. Mazloomi, S. K., & Sulaiman, N. (2012). Influencing factors of water electrolysis electrical efficiency. In *Renewable and Sustainable Energy Reviews* 16(6) 4257–4263. https://doi.org/10.1016/j.rser.2012.03.052
51. Kalinci, Y., Hepbasli, A., & Dincer, I. (2009). Biomass-based hydrogen production: A review and analysis. In *International Journal of Hydrogen Energy* 34(21) 8799–8817. https://doi.org/10.1016/j.ijhydene.2009.08.078
52. Sharma, S., & Ghoshal, S. K. (2015). Hydrogen the future transportation fuel: From production to applications. In *Renewable and Sustainable Energy Reviews* 43, 1151–1158. Elsevier Ltd. https://doi.org/10.1016/j.rser.2014.11.093
53. Wang, R. R., Zhao. Y.Q., Babich, A., Senk, D., & Fan, X. Y. (2021). Hydrogen direct reduction (H-DR) in steel industry—An overview of challenges and opportunities. *Journal of Cleaner Production*, *329*(129799), 1–10. https://doi.org/10.1016/j.jclepro.2021.129797
54. BMWK, "National Hydrogen Strategy Update," Berlin, Jul. 2023. [Online]. Accessed: Jan. 18, 2024. Available: www.bmwk.de
55. World Steel Association, "Hydrogen (H2)-based ironmaking Fact sheet," 2021. [Online]. Accessed: Mar. 5, 2023. Available: https://fuelcellsworks.com/news/worlds-largest-hydrogen-plant-in-fukushima-opens/
56. Ye, L., Peng, Z., Wang, L., Anzulevich, A., Bychkov, I., Kalganov, D., Tang, H., Rao, M., Li, G., & Jiang, T. (2019). Use of Biochar for Sustainable Ferrous Metallurgy. *JOM*, *71*(11), 3931–3940. https://doi.org/10.1007/s11837-019-03766-4
57. Adrados, A., De Marco, I., López-Urionabarrenechea, A., Solar, J., Caballero, B. M., & Gastelu, N. (2016). Biomass pyrolysis solids as reducing agents: Comparison with commercial reducing agents. *Materials*, *9*(1). https://doi.org/10.3390/ma9010003
58. Zulkania, A., Rochmadi, R., Hidayat, M., & Cahyono, R. B. (2022). Reduction Reactivity of Low Grade Iron Ore-Biomass Pellets for a Sustainable Ironmaking Process. *Energies*, *15*(1). https://doi.org/10.3390/en15010137
59. Suopajärvi, H., Pongrácz, E., & Fabritius, T. (2013). The potential of using biomass-based reducing agents in the blast furnace: A review of thermochemical conversion technologies and assessments related to sustainability. *Renewable and Sustainable Energy Reviews*, *25*, 511–528. https://doi.org/10.1016/j.rser.2013.05.005
60. Mousa, E., Wang, C., Riesbeck, J., & Larsson, M. (2016). Biomass applications in iron and steel industry: An overview of challenges and opportunities. *Renewable and Sustainable Energy Reviews*, *65*, 1247–1266. https://doi.org/10.1016/j.rser.2016.07.061
61. Kumar, U., Maroufi, S., Rajarao, R., Mayyas, M., Mansuri, I., Joshi, R. K., & Sahajwalla, V. (2017). Cleaner production of iron by using waste macadamia biomass as a carbon resource. *Journal of Cleaner Production*, *158*, 218–224. https://doi.org/10.1016/j.jclepro.2017.04.115
62. Zhou, S., Wei, Y., Li, B., & Wang, H. (2019). Cleaner recycling of iron from waste copper slag by using walnut shell char as green reductant. *Journal of Cleaner Production*, *217*, 423–431. https://doi.org/10.1016/j.jclepro.2019.01.184
63. Zuo, H. Bin, Hu, Z. W., Zhang, J. L., Li, J., & Liu, Z. J. (2013). Direct reduction of iron ore by biomass char. *International Journal of Minerals, Metallurgy and Materials*, *20*(6), 514–521. https://doi.org/10.1007/s12613-013-0759-7
64. Hidayanti, R., Permana, S., Maksum, A., & Soedarsono, J. W. (2018). Study on the effects of temperature in the carbothermic reduction laterite ore using palm kernel shell as reducing agent. *IOP Conference Series: Earth and Environmental Science*, *105*(1). https://doi.org/10.1088/1755-1315/105/1/012015

65. Avarmaa, K., Järvenpää, M., Klemettinen, L., Marjakoski, M., Taskinen, P., Lindberg, D., & Jokilaakso, A. (2020). Battery scrap and biochar utilization for improved metal recoveries in nickel slag cleaning conditions. *Batteries*, *6*(4), 1–21. https://doi.org/10.3390/batteries6040058
66. Bagatini, M. C., Kan, T., Evans, T. J., & Strezov, V. (2021). Iron Ore Reduction by Biomass Volatiles. *Journal of Sustainable Metallurgy*, *7*(1), 215–226. https://doi.org/10.1007/s40831-021-00337-3
67. Wang, Q., Zhang, B., Yu, S., Xiong, J., Yao, Z., Hu, B., & Yan, J. (2020). Waste-Printed Circuit Board Recycling: Focusing on Preparing Polymer Composites and Geopolymers. In *ACS Omega.* 5(29), 17850–17856. https://doi.org/10.1021/acsomega.0c01884
68. Zhao, W., Xu, J., Fei, W., Liu, Z., He, W., & Li, G. (2022). The reuse of electronic components from waste printed circuit boards: a critical review. In *Environmental Science: Advances* 2(2) 196–214). https://doi.org/10.1039/d2va00266c
69. Cucchiella, F., D'Adamo, I., Lenny Koh, S. C., & Rosa, P. (2015). Recycling of WEEEs: An economic assessment of present and future e-waste streams. In *Renewable and Sustainable Energy Reviews* 51, 263–272. https://doi.org/10.1016/j.rser.2015.06.010
70. Tesfaye, F., Lindberg, D., Hamuyuni, J., Taskinen, P., & Hupa, L. (2017). Improving urban mining practices for optimal recovery of resources from e-waste. *Minerals Engineering*, *111*, 209–221. https://doi.org/10.1016/j.mineng.2017.06.018
71. Forti, V., Baldé, C. P., Kuehr, R., & Bel, G. (2020). *The Global E-waste Monitor 2020*.
72. Duan, H., Hou, K., Li, J., & Zhu, X. (2011). Examining the technology acceptance for dismantling of waste printed circuit boards in light of recycling and environmental concerns. In *Journal of Environmental Management* 92(3), 392–399. https://doi.org/10.1016/j.jenvman.2010.10.057
73. Ghosh, B., Ghosh, M. K., Parhi, P., Mukherjee, P. S., & Mishra, B. K. (2015). Waste Printed Circuit Boards recycling: An extensive assessment of current status. In *Journal of Cleaner Production* 94, 5–19). Elsevier Ltd. https://doi.org/10.1016/j.jclepro.2015.02.024
74. Cui, H., & Anderson, C. (2016). Literature Review of Hydrometallurgical Recycling of Printed Circuit Boards (PCBs). *Journal of Advanced Chemical Engineering*, *6*(1). https://doi.org/10.4172/2090-4568.1000142
75. D'Adamo, I., Ferella, F., Gastaldi, M., Maggiore, F., Rosa, P., & Terzi, S. (2019). Towards sustainable recycling processes: Wasted printed circuit boards as a source of economic opportunities. *Resources, Conservation and Recycling*, *149*, 455–467. https://doi.org/10.1016/j.resconrec.2019.06.012
76. Khaliq, A., Rhamdhani, M. A., Brooks, G., & Masood, S. (2014). Metal extraction processes for electronic waste and existing industrial routes: A review and Australian perspective. In *Resources* 3(1), 152–179). https://doi.org/10.3390/resources3010152
77. Ahirwar, R., & Tripathi, A. K. (2021). E-waste management: A review of recycling process, environmental and occupational health hazards, and potential solutions. In *Environmental Nanotechnology, Monitoring and Management* 15. Elsevier B.V. https://doi.org/10.1016/j.enmm.2020.100409
78. Zulkernain, N. H., Basant, N., Ng, C. C., Kriti, Salari, M., & Mallick, S. (2023). Recovery of precious metals from e-wastes through conventional and phytoremediation treatment methods: a review and prediction. In *Journal of Material Cycles and Waste Management* 25(5), 2726–2752. https://doi.org/10.1007/s10163-023-01717-5
79. Rene, E. R., Sethurajan, M., Kumar Ponnusamy, V., Kumar, G., Bao Dung, T. N., Brindhadevi, K., & Pugazhendhi, A. (2021). Electronic waste generation, recycling and resource recovery: Technological perspectives and trends. *Journal of Hazardous Materials*, *416*. https://doi.org/10.1016/j.jhazmat.2021.125664
80. Sohaili, J., Kumari Muniyandi, S., & Suhaila Mohamad, S. (2012). A Review on Printed Circuit Boards Waste Recycling Technologies and Reuse of Recovered Nonmetallic Materials. *International Journal of Scientific & Engineering Research*, *3*(2). http://www.ijser.org

81. Babich, A., Senk, D., Knepper, M., & Benkert, S. (2016). Conversion of injected waste plastics in blast furnace. *Ironmaking and Steelmaking*, *43*(1), 11–21. https://doi.org/10.1179/1743281215Y.0000000042
82. Carpenter, A. M. (2010). Injection of coal and waste plastics in blast furnaces. In *IEA Clean Coal Centre*. IEA Clean Coal Centre.
83. Murakami, T., & Kasai, E. (2011). Reduction mechanism of iron oxide-carbon composite with polyethylene at lower temperature. *ISIJ International*, *51*(1), 9–13. https://doi.org/https://doi.org/10.2355/isijinternational.51.9
84. Sahajwalla, V., Zaharia, M., Kongkarat, S., Khanna, R., Saha-Chaudhury, N., & O'Kane, P. (2010). Recycling plastics as a resource for electric arc furnace (EAF) steelmaking: Combustion and structural transformations of metallurgical coke and plastic blends. *Energy and Fuels*, *24*(1), 379–391. https://doi.org/10.1021/ef900875r
85. Ziebik, A., & Stanek, W. (2001). Forecasting of the energy effects of injecting plastic wastes into the blast furnace in comparison with other auxiliary fuels. In *Energy*. 26.
86. Lotfian, S., Ahmed, H., & Samuelsson, C. (2017). Alternative Reducing Agents in Metallurgical Processes: Devolatilization of Shredder Residue Materials. *Journal of Sustainable Metallurgy*, *3*(2), 311–321. https://doi.org/10.1007/s40831-016-0094-0
87. Dankwah, J. R., Amoah, T., Dankwah, J., & Fosu Dankwah, A. Y. (2015). Recycling Mixed Plastics Waste as Reductant in Ironmaking. In *Ghana Mining Journal* 15(2).
88. Wang, G., Wang, J., & Xue, Q. (2020). Efficient utilization of waste plastics as raw material for metallic iron and syngas production by combining heat treatment pulverization and direct reduction. *Process Safety and Environmental Protection*, *137*, 49–57. https://doi.org/10.1016/j.psep.2020.02.017
89. Zhang, J., Fu, H., Liu, Y., Dang, H., Ye, L., Conejio, A. N., & Xu, R. (2022). Review on biomass metallurgy: Pretreatment technology, metallurgical mechanism and process design. *International Journal of Minerals, Metallurgy and Materials*, *29*(6), 1133–1149. https://doi.org/10.1007/s12613-022-2501-9
90. Koskela, A., Heikkilä, A., Bergna, D., Salminen, J., & Fabritius, T. (2021). Effects of briquetting and high pyrolysis temperature on hydrolysis lignin char properties and reactivity in co-co2-n2 conditions. *Minerals*, *11*(2), 1–17. https://doi.org/10.3390/min11020187
91. Hellstén, N., Klemettinen, L., Sukhomlinov, D., O'Brien, H., Taskinen, P., Jokilaakso, A., & Salminen, J. (2019). Slag Cleaning Equilibria in Iron Silicate Slag–Copper Systems. *Journal of Sustainable Metallurgy*, *5*(4), 463–473. https://doi.org/10.1007/s40831-019-00237-7
92. Pouchou, J. L., & Pichoir, F. (1986) "Basic expression of 'PAP' computation for quantitative EPMA," in *Proceedings of the 11th International Congress on X ray Optics and Microanalysis*, Brown J D and Packwood R H, Eds., London, 249–256.
93. Van Achterbergh, E., Ryan, C. G., Jackson, S. E., & Griffin, W. L. (2001) *Data reduction software for LA-ICP-MS*, Sylvester P J., vol. 29. Ottawa, Ontario: Mineralogical Association of Canada
94. Jochum K. P., Nohl, U., Herwig, K., Lammel, E., Stoll, B., & Hofmann, A.W. (2005) "GeoReM: A new geochemical database for reference materials and isotopic standards," *Geostand Geoanal Res*, 29(3) 333–338. https://doi.org10.1111/j.1751-908x.2005.tb00904.x.
95. Bale, C. W., Bélisle, E., Chartrand, P., Decterov, S. A., Eriksson, G., Gheribi, A. E., Hack, K., Jung, I., Kang, Y., Melançon, J., Pelton, A. D., Petersen, S., Robelin, C., Sangster, J., Spencer, P., & Ende, M. Van. (2016). CALPHAD : Computer Coupling of Phase Diagrams and Thermochemistry FactSage thermochemical software and databases , 2010 – 2016. *Calphad*, *54*, 35–53. https://doi.org/10.1016/j.calphad.2016.05.002
96. Kleynhans, E. L. J., Beukes, J. P., Van Zyl, P. G., Bunt, J. R., Nkosi, N. S. B., & Venter, M. (2017). The Effect of Carbonaceous Reductant Selection on Chromite Pre-reduction. *Metallurgical and*

Materials Transactions B: Process Metallurgy and Materials Processing Science, *48*(2), 827–840. https://doi.org/10.1007/s11663-016-0878-4

97. Li, J., Duan, H., Yu, K., Liu, L., & Wang, S. (2010). Characteristic of low-temperature pyrolysis of printed circuit boards subjected to various atmosphere. *Resources, Conservation and Recycling*, *54*(11), 810–815. https://doi.org/10.1016/j.resconrec.2009.12.011
98. Rajagopal, R. R., Rajarao, R., & Sahajwalla, V. (2016). High temperature transformations of waste printed circuit boards from computer monitor and CPU: Characterisation of residues and kinetic studies. *Waste Management*, *57*, 91–101. https://doi.org/10.1016/j.wasman.2015.11.016
99. Jung, S. M., & Yi, S. H. (2013). A kinetic study on carbothermic reduction of hematite with graphite employing thermogravimetry and quadruple mass spectrometry. *Steel Research International*, *84*(9), 908–916. https://doi.org/10.1002/srin.201200310
100. Nurmi, S. (2018). *Experimental Study of Speiss Formation in Reductive Thermal Treatment of Jarosite Residue*. Aalto University.
101. Rinne, M. (2019). *Pyrometallurgical treatment of jarosite leach residue by non-fossil reductant*. Aalto University.
102. Chaidez-Felix, J., Romero-Serrano, A., Hernandez-Ramirez, A., Perez-Labra, M., Almaguer-Guzman, I., Benavides-Perez, R., & Flores-Favela, M. (2014). Effect of copper , sulfur , arsenic and antimony on silver distribution in phases of lead blast furnace. *Transactions of Nonferrous Metals Society of China*, *24*(4), 1202–1209. https://doi.org/10.1016/S1003-6326(14)63180-0
103. Lahijani, P., Zainal, Z. A., Mohammadi, M., & Mohamed, A. R. (2015). Conversion of the greenhouse gas CO2 to the fuel gas CO via the Boudouard reaction: A review. *Renewable and Sustainable Energy Reviews*, *41*, 615–632. https://doi.org/10.1016/j.rser.2014.08.034
104. Dańczak, A., Ruismäki, R., Rinne, T., Klemettinen, L., O'brien, H., Taskinen, P., Jokilaakso, A., & Serna-guerrero, R. (2021). Worth from waste: Utilizing a graphite-rich fraction from spent lithium-ion batteries as alternative reductant in nickel slag cleaning. *Minerals*, *11*(7). https://doi.org/10.3390/min11070784
105. Rinne, T., Klemettinen, A., Klemettinen, L., Ruismäki, R., O'brien, H., Jokilaakso, A., & Serna-Guerrero, R. (2022). Recovering value from end-of-life batteries by integrating froth flotation and pyrometallurgical copper-slag cleaning. *Metals*, *12*(1). https://doi.org/10.3390/met12010015

Aalto-DT 283/2024

ISBN 978-952-64-2209-1 (printed)
ISBN 978-952-64-2210-7 (pdf)
ISSN 1799-4934 (printed)
ISSN 1799-4942 (pdf)

Aalto University
School of Chemical Engineering
Department of Chemical and Metallurgical Engineering
www.aalto.fi

BUSINESS + ECONOMY

ART + DESIGN + ARCHITECTURE

SCIENCE + TECHNOLOGY

CROSSOVER

DOCTORAL THESES